# Sensing transport: label-free in vitro assays as an atTRACTive alternative for solute carrier transporter drug discovery

Sijben, H.J.

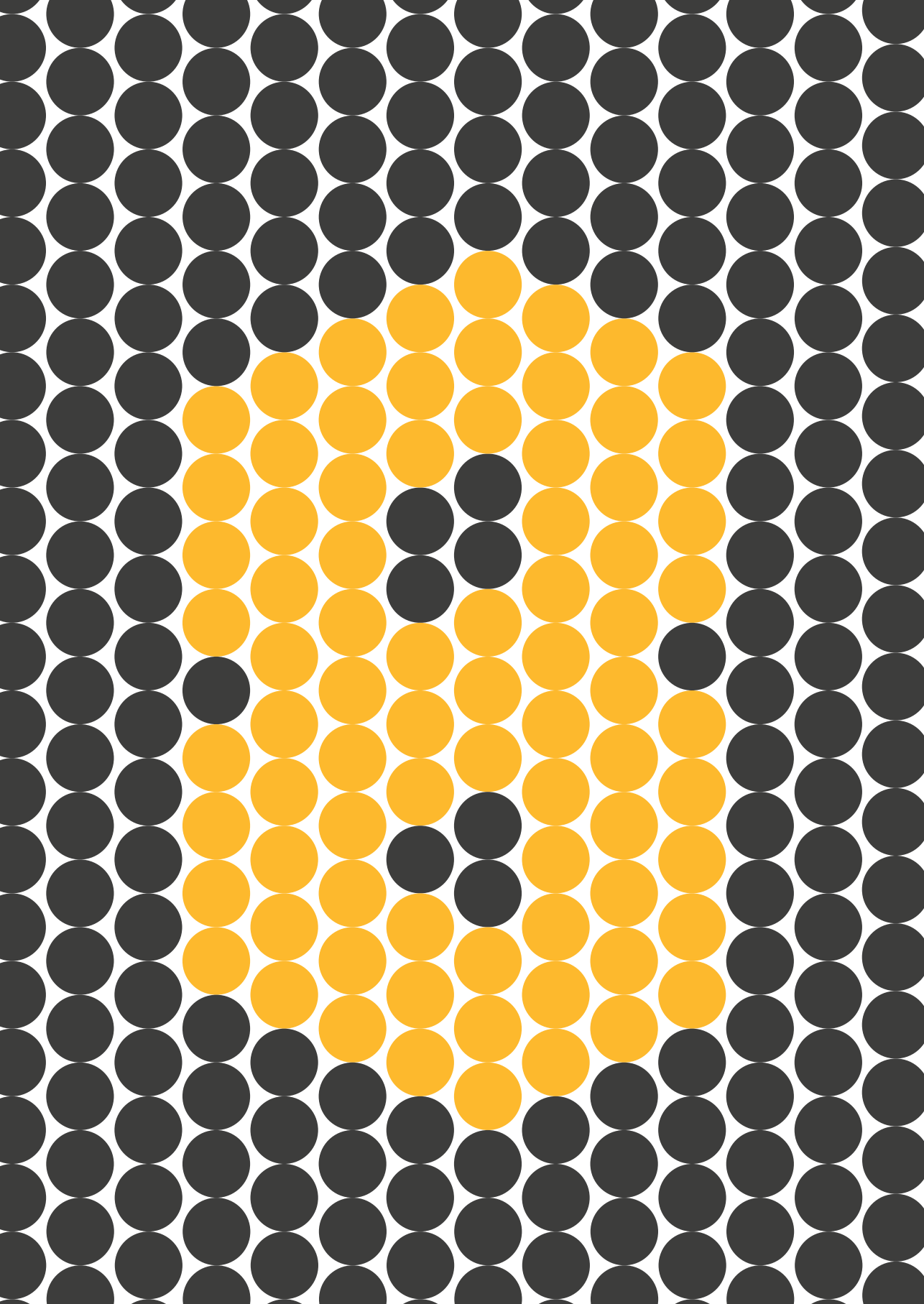

# CHAPTER 8

# General discussion, conclusions and future perspectives

The ubiquitous presence of solute carrier (SLC) transporters makes them indispensable in many physiological processes. When these transport proteins are dysfunctional, however, they can cause or contribute to the development of diseases. In the search towards effective therapeutics that directly or indirectly modulate the function of SLCs, it is crucial to have access to robust and reliable *in vitro* assays that can help identify substrates, inhibitors and modulators. The chapters in this thesis describe the exploration, development, validation and application of two novel types of transporter assays, which are based on the use of a label-free, impedance-based technology. The main results and conclusions of these studies will be summarized and discussed in the following sections. The findings will be put in perspective of traditional concepts and the future of label-free assays in SLC research will be speculated on. Ultimately, this thesis advocates the impedance-based label-free technology as the 'new kid on the block' of SLC assays and marks the advent of a novel method to investigate this protein family.

**General discussion and conclusions**

In order to check whether a molecule possesses any biological activity that may alleviate a patient's symptoms or prevent disease phenotypes, we need assays that mimic a biological system in which the molecule may be active. Prior to testing any molecule in live organisms – be it zebrafish or humans – we would need to know upfront whether that molecule can engage the intended target (e.g., receptor or transporter) and evokes the intended response (i.e., activation or inhibition), preferably with good pharmacokinetic properties and limited off-target toxicity. Computational models, such as the ones described in **Chapter 4**, have become increasingly powerful tools in the prediction of a molecule's activity at any biological target, which can be used to conceive previously unimagined molecular scaffolds and select candidate molecules for *in vitro* testing in an early stage of drug discovery[1,2]. Although these computational approaches can help to cut the amount of labor-intensive wet-lab tests, the predicted molecules still need to be tested for their activity on the physical target of interest.

## 8.1 – The added value of cell-based label-free assays

Numerous *in vitro* model systems have been developed to test molecules and address a wide range of pharmacological research questions in various stages of the drug discovery process, being based on the use of cells (e.g., heterologous bacteria/yeast/mammalian cells, primary cells, organoids, 'organ-on-a-chip'[3–5]) or cell-free preparations (e.g., cell extracts, membranes, purified or engineered protein[6,7]). Where some systems allow a detailed detection and/or visualization of physiological events upon treatment, there is always a trade-off in terms of throughput (i.e., the number of molecules that can be tested within a specified time), running costs per sample, complexity of data analysis/interpretation and physiological relevance. In **Chapter 1**, the advantages and limitations of established techniques and model systems for solute carrier (SLC) transporters are summarized with regard to their trade-offs (**Table 1.1**). The main conclusion of this summary is that the current SLC assays are either label-based, low in throughput, incompatible with live cells and/or unable to perform real-time measurements. If high-throughput screening (HTS) of molecules in a closer-to-physiology setting is to the benefit of successful translational drug discovery, then there is a need for alternative assay strategies to aid in this process. Thus, cell-based label-free assays are an attractive approach to assess target pharmacology in live cells without the use of cell-intrusive and non-physiological chemical labels.

Cell-based label-free assays offer an advantage over conventional biochemical assays – in addition to offering increased physiological relevance[8] – in that they are able to capture the sum of events that follow a perturbation of the cell (e.g., receptor activation or the uptake of cytotoxic compounds) in real-time, instead of focusing on a single pathway downstream of this perturbation (e.g., cAMP production, protein phosphorylation or apoptosis markers) at a fixed point in time[9,10]. It is this characteristic of cell-based label-free assays that is at the basis of the assays that are described in the chapters of this thesis. The impedance-based biosensor xCELLigence has previously been used to detect changes in cells' morphology as a result of the activation of G protein-coupled receptors (GPCRs)

that are expressed on these cells[11,12]. The intracellular signaling events that are triggered upon GPCR activation lead to ordered and dynamic rearrangement of the cytoskeleton and redistribution of proteins and organelles, which can be interpreted as the functional or phenotypic effect of receptor activation[12,13]. For example, adenosine receptors (ARs) are activated by their endogenous ligand, adenosine, and several studies demonstrate that activation of subtypes of these receptors ($A_1AR$[14], $A_{2A}AR$[15], $A_{2B}AR$[16]) by adenosine or other agonists leads to temporary contraction, spreading or shrinkage of the cells, which can be deduced from the real-time changes in electrical impedance – expressed as the Cell Index (CI) – that are recorded by the xCELLigence. Thus, the xCELLigence is able to 'sense' the presence of a ligand (i.e., agonist) by using cells that express a receptor that is specific to this ligand. Moreover, the sensors are highly sensitive, meaning that they can pick up signals even in conditions where the expression levels of the protein are very low (e.g., in cells with endogenous receptor expression)[17,18] or the adhesion of the cells to the E-plate is poor[19]. By exploiting this sensitivity, the xCELLigence can be used to detect minute changes in agonist concentration.

### 8.2 – Transporters can affect the concentration of agonists at the receptor compartment

The extracellular concentration of an agonist is dictated by distinct (non-)physiological processes including enzymatic degradation or biosynthesis of the ligand[20], adsorption of the ligand to biological membranes or plastics (i.e., non-specific binding[21]), excretion or efflux of the ligand from cells or uptake of the ligand into cells *via* transporters[22]. While it is common to mitigate processes that influence the ligand concentration – e.g., by inhibition or expression of enzymes or transporters – to benefit proper assessment of receptor pharmacology, until recently there had been no reports that exploited the activation of membrane receptors to primarily investigate such processes.

Prior to the conception of the projects that are described in this thesis, it was demonstrated by colleagues that the presence of the equilibrative nucleoside transporter 1 (ENT1/SLC29A1) – a bidirectional transporter of adenosine – on an osteosarcoma cell line (U2OS) resulted in an attenuated activation of the endogenously expressed $A_{2B}AR$ by adenosine, which was measured using xCELLigence[23]. This attenuation was likely the result of partial removal of the added adenosine from the extracellular compartment by ENT1. Indeed, when cells were pretreated with inhibitors of ENT1 (e.g. dipyridamole, NBTI) the apparent potency of adenosine for $A_{2B}AR$ was increased (i.e., shifted leftward) up to ten-fold, which suggested that adenosine uptake skewed the pharmacology of the endogenous agonist causing an underestimation of its potency. In this regard the cells are able to detect the reduced agonist availability at the receptor compartment, which can be interpreted as a direct causality of ENT1 function. As such, the xCELLigence is 'sensing transport', which offers the possibility to assess the pharmacology of molecules that modulate the transporter. For the purpose of naming simplification, we have termed the resulting method based on this concept the '**transport activity through receptor activation**' (**TRACT**) assay (**Chapter**

**3**), which in this thesis refers to the xCELLigence-based assays but could more generally refer to any assay that uses receptor activation as a readout to determine transporter activity (e.g., $Ca^{2+}$ mobilization, GTPγS, cAMP or β-arrestin assays[24]).

ENT1 is certainly not the only transporter that modulates agonist availability for membrane receptors (**Chapter 2**). In fact, a thorough assessment of the literature and pharmacology databases suggest that there are at least 100 unique human SLCs that are involved in the translocation of a substrate that is also a receptor agonist (**Appendix, Table A.1**). The majority of these SLCs are located at the plasma membrane, although some (mainly vesicular neurotransmitter transporters) are located at intracellular compartments. A few of these SLCs are well-known modulators of agonist levels and are common therapeutic targets – e.g., monoamine transporters (DAT, NET, SERT) decrease synaptic levels of monoamine neurotransmitters, where antidepressants primarily inhibit reuptake to enhance neurotransmitter levels, potentiate stimulatory receptor signaling and alleviate depression[25–27]. Although these SLCs mostly operate to *reduce* extracellular agonist levels, in **Chapter 2** we advocate SLCs that have been recently demonstrated to *increase* extracellular levels of agonist *via* efflux, such as the sphingosine-1-phosphate transporter (SPNS2/SLC63A2)[28] and succinate efflux *via* the monocarboxylate transporter 1 (MCT1/SLC16A1)[29]. In addition, SLCs may provide GPCRs located at intracellular membranes with their cognate ligands *via* influx, adding another layer of activation control by transporters. As is exemplified by the extensive **Table A.1**, there are many SLCs that can be 'linked' to a receptor *via* its substrate(s), which provides ample opportunities for label-free assay development (see **section 8.9**). Thus, we commenced by investigating which SLCs – other than ENT1 – would be suitable for functional assessment using the xCELLigence.

### 8.3 – Development of the TRACT assay for DAT, NET and EAAT

In this thesis, we focus on human SLCs that upon exogenous substrate application mediate substrate influx, i.e. remove the agonist from the receptor compartment. To start the validation of the impedance-based assay for other transporters, we initially selected SLCs that are well-studied and clinically relevant, have known substrate(s) ascribed to them and for which several validated small molecule inhibitors are available. We then identified an SLC and GPCR 'pair' that shared the same substrate. An important factor to consider was that the SLC and GPCR should be expressed on the same cell to facilitate sufficient removal of the substrate from the proximity of receptor compartment, similar to the study by Vlachodimou *et al.* in which cells were used with endogenous expression of both ENT1 and ARs[23]. This, however, will not always be the case and in such instances where only the SLC or GPCR is expressed by the cell – or, if both are lacking – it is necessary to induce heterologous expression of the 'missing' protein(s) *via* transient or stable transfection of the transgene. Based on these prerequisites, three SLCs with GPCR-activating substrates were selected as 'model' SLCs for proof-of-concept validations of the impedance-based assay: the dopamine transporter (DAT/SLC6A2), norepinephrine transporter (NET/SLC6A2) and the excitatory amino acid transporter 1 (EAAT1/SLC1A3).

The functionality of human DAT was the first to be assessed on xCELLigence (**Chapter 3**). DAT is a well-established target of psychostimulants such as amphetamines and cocaine, as well as drugs for the treatment of depression, ADHD, narcolepsy and stimulant abuse[26]. Thus, we selected DAT as a model SLC to validate our assay hypothesis. To this end, the human osteosarcoma U2OS cell line was selected as a model system as they are adherent – which is important for proper detection of impedance changes[30] – and endogenously express the dopamine receptor D1 ($D_1R$). Since these cells did not express DAT, we transiently transfected the U2OS cells with SLC6A3 or mock DNA prior to treatment of the cells with the endogenous substrate dopamine. As expected, the apparent potency of dopamine at $D_1R$ was decreased in the presence of DAT and was potentiated when cells were pretreated with the DAT inhibitor GBR12909, which indicated that dopamine was efficiently removed from the extracellular compartment by DAT[31]. These findings were in line with the previously mentioned adenosine/ENT1 experiments and allowed for the determination of the inhibitory potency of GBR12909.

Although the TRACT assay principle was demonstrated in U2OS cells, the transient transfection procedure was deemed unsuitable for screening purposes and could be subject to inter-experimental variability of transporter expression levels. To attain stable transporter expression levels throughout experiments, we introduced the use of an engineered human embryonic kidney 293 (HEK293) cell line with stable site-specific integration of the transporter gene into the cell's genome, which allows for doxycycline-inducible expression of the transporter under a tetracycline repressor[32]. Since non-induced cells display little to no transporter expression, these cells can act as negative control to the induced, overexpressing cells. A major advantage of this so-called JumpIn system is the homogenous, consistent and high expression levels of the gene, which leads to more reproducible data across labs and experiments[33]. In addition, the time required to generate JumpIn pools (~3 weeks) is considerably shorter and less error-prone than that to isolate stable monoclonal cells (~3 months), which facilitates the rapid generation of multiple JumpIn cell lines with different transporters or with genetic variants of the transporters (as is shown for EAAT1 mutants in **Chapter 7**). Thus, JumpIn cells were used for nearly all subsequent experiments and proved to be a valuable and easy-to-use tool for the set-up and validation of impedance-based transporter assays.

To demonstrate the compatibility of JumpIn cells, we used the TRACT assay in U2OS-DAT cells as a starting point for similar experiments on JumpIn cells expressing DAT (JumpIn-

→ **Figure 8.1** – Proposed workflow for TRACT assay development. **Top**: a 'toolbox' should be assembled, consisting of: an SLC–GPCR pair; substrate(s) and inhibitors; a cell line that expresses both SLC and GPCR; a control cell line that lacks the SLC. **Middle**: cell seeding density and assay conditions (e.g., buffer composition, incubation time) should be optimized to maximize the response window. This is followed by determination of the substrate potency in the presence and absence of the SLC, and a pharmacological validation of the GPCR or pathway that is involved in the substrate response. **Bottom**: the substrate response is determined in the presence of an SLC inhibitor, which provides an assay window to determine the inhibitory potency. The resulting assay should be validated to adhere to high-throughput screening (HTS) criteria, after which it can be used for compound screening.

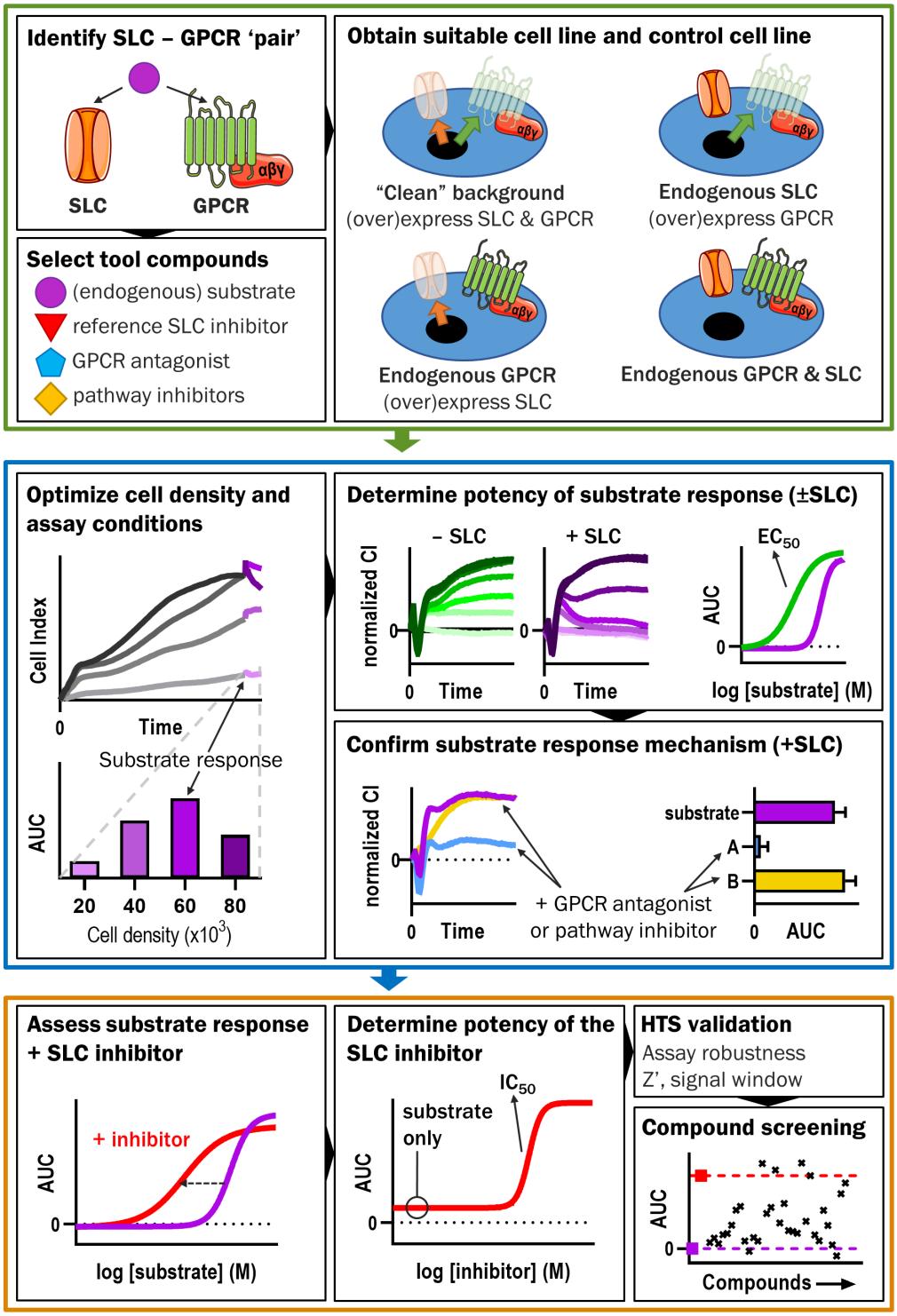
Identify SLC – GPCR 'pair'
SLC
GPCR
αβγ
Select tool compounds
(endogenous) substrate
reference SLC inhibitor
GPCR antagonist
pathway inhibitors
Obtain suitable cell line and control cell line
"Clean" background
(over)express SLC & GPCR
Endogenous SLC
(over)express GPCR
Endogenous GPCR
(over)express SLC
Endogenous GPCR & SLC
Optimize cell density and assay conditions
Cell Index
Time
Substrate response
AUC
20 40 60 80
Cell density (x10^3)
Determine potency of substrate response (±SLC)
– SLC
+ SLC
normalized CI
Time
EC50
AUC
log [substrate] (M)
Confirm substrate response mechanism (+SLC)
normalized CI
Time
+ GPCR antagonist
or pathway inhibitor
substrate
A
B
AUC
Assess substrate response + SLC inhibitor
+ inhibitor
AUC
log [substrate] (M)
Determine potency of the SLC inhibitor
IC50
substrate only
AUC
log [inhibitor] (M)
HTS validation
Assay robustness
Z', signal window
Compound screening
AUC
Compounds

DAT) (**Chapter 3**). Although the JumpIn cells did not express endogenous dopamine receptors, we observed dopamine induced concentration-dependent cellular responses that were attributed to the activation of alpha-2 adrenergic receptors ($\alpha_2$R). Upon induction of DAT expression, the apparent potency of dopamine was significantly reduced, which was rescued by both GBR12909 and cocaine with the inhibitory potency of GBR12909 being comparable between U2OS and JumpIn cells. This indicated that receptors with differential intracellular G protein-coupling ($G_{\alpha s}$ for $D_1$R, $G_{\alpha i}$ for $\alpha_2$R) and similar agonist potencies were both affected by the presence of an agonist uptake process.

In **Chapter 4**, we extended the TRACT assay principle to study NET, which is a drug target for depression and ADHD, and has an overlapping pharmacology with DAT[26]. We used JumpIn cells with inducible expression of NET (JumpIn-NET), which were responsive to norepinephrine *via* activation of endogenous $\alpha_2$R. Dopamine and epinephrine, which are both NET substrates, also induced $\alpha_2$R-mediated cellular responses. The apparent potency of all three substrates was decreased in the presence of NET, with the shift being largest for norepinephrine (16-fold) and smallest for dopamine (3-fold). Moreover, the responses of all substrates were restored equipotently by NET inhibitor nisoxetine, where norepinephrine displayed the largest assay window (i.e., signal-to-noise ratio). The inhibitory potencies of twelve well-known NET inhibitors were in good correlation with a conventional fluorescent substrate uptake assay over a wide range of potencies, suggesting that the TRACT assay can be used to accurately characterize inhibitors. The Z' factor – which is a parameter of assay robustness and reproducibility used in HTS[34] – for this assay was 0.55, which is sufficient to deem the assay suitable for compound screening.

In **Chapter 6**, we attempted to set-up a TRACT assay for EAAT1, which mediates uptake of glutamate in astrocytes of the central nervous system and shows promise as a drug target for neurological disorders that involve glutamate homeostasis, such as epilepsy, ataxia and schizophrenia[35]. As JumpIn cells do not express glutamate receptors, we performed experiments with JumpIn-EAAT1 cells transiently transfected with the metabotropic glutamate receptor 2 ($mGluR_2$), as we had in-house experience with $mGluR_2$ functional assays on xCELLigence[36]. In non-induced cells, L-glutamate induced an $mGluR_2$-mediated response within 15 minutes, although the potency was substantially lower ($pEC_{50}$ = 4.1) than previously reported for human $mGluR_2$ expressed heterologously in Chinese hamster ovary (CHO) cells on xCELLigence ($pEC_{50}$ = 5.3)[37], which could be due to the transfection method (transient versus stable)[38] or cellular background (i.e., system bias)[39]. Nevertheless, induced EAAT1 expression attenuated the L-glutamate response at $mGluR_2$, causing a rightward shift of the concentration-effect curve. The allosteric EAAT1 inhibitor UCPH-101 restored the apparent potency of L-glutamate on $mGluR_2$, but the more potent competitive inhibitor TFB-TBOA prevented all L-glutamate-induced responses. As a result, we were unable to reliably determine inhibitory potencies in the TRACT assay using this particular set-up. Interestingly, at high L-glutamate concentrations (>100 μM) a substantial $mGluR_2$-independent cellular response was observed that was attributed to cell swelling and spreading, providing an alternative assay window which we will discuss further in **section 8.6**.

Taken together, we demonstrated the TRACT assay principle for three human SLCs in a versatile JumpIn cell line, of which Gateway-compatible expression vectors are commercially available *via* Addgene (http://www.addgene.org/depositor-collections/re-solute/). In theory, any SLC–GPCR 'pair' that recognizes the same substrate is amenable for a TRACT assay. We have provided a visual workflow based on the assay development in **Chapter 3, 4 and 6**, which can be used as a guideline to set-up the TRACT assay for other SLCs (**Figure 8.1**). In the following section, we attempt to provide a rationale for a successful TRACT assay based on properties of the transporter and the receptor.

### 8.4 – A mechanistic understanding of the TRACT assay

In order to rationally approach the design of TRACT assays for new SLCs we would need to identify the key parameters that should match between the SLC and GPCR in order to ensure that the substrate uptake sufficiently affects the receptor occupancy. From a physiological perspective, it can be rationalized that saturable uptake processes are essential to remove excessive amounts of agonist from the receptor compartment to control the level of receptor activation. The initial recognition of these concepts originates from early denervation experiments in which removal of nerves from cholinergic or adrenergic tissue in humans or animals caused an increased responsiveness or sensitivity of the tissue to the corresponding neurotransmitter. In 1939, this was formulated by Walter Bradford Cannon as the 'Law of Denervation': "*When in a series of efferent neurons a unit is destroyed, an increased irritability to chemical agents develops in the isolated structure or structures, the effect being maximal in the part directly denervated.*"[40]. This phenomenon was termed 'supersensitivity' and could be attained either by denervation of the tissue or pharmacological treatment with substances that enhance neurotransmitter sensitivity, such as cocaine[41]. In essence, the nerves were found to be responsible for the timely removal (i.e., uptake) of released neurotransmitters, which lowered the availability of the neurotransmitter to the postsynaptic tissue. It was not until the early 1960's that researchers identified active uptake mechanisms that were saturable and adhered to Michaelis-Menten kinetics[42–44], suggesting the involvement of high-affinity (i.e., $uptake_1$, now known as neuronal NET, DAT and SERT[26]) and low-affinity carriers ($uptake_2$, identified as the non-neuronal organic cation transporters [OCT1–3, SLC22A1–3][45], and the plasma membrane monoamine transporter [PMAT, SLC29A4][46]) for the removal of released neurotransmitters.

It was soon found that uptake processes could lead to an underestimation of the true potency of an agonist and that action should be taken to prevent substantial influence of uptake on receptor activation. For example, by blocking $uptake_1$ cocaine sensitizes the activation of adrenergic receptors, 'revealing' the potency of norepinephrine[22,47]. Likewise, the ENT1 inhibitor NBMPR (or NBTI) was used to prevent uptake of adenosine, which enhanced the potency of adenosine at AR subtypes in a cAMP assay[48]. In another scenario, uptake of endogenous ligand is desired so that it does not disturb the pharmacological characterization of compounds at that ligand's receptor. Since glutamate is present in cell culture medium and is continuously produced by cells[36,49], some experimental set-ups

warrant the co-expression of EAATs on mGluR-expressing cells to deplete the endogenous glutamate so it does not interfere with mGluR activation by exogenous agonists[50]. These findings are at the basis of the TRACT assay principle that is described in this thesis.

If the aforementioned uptake processes are able to remove sufficient amounts of substrate from the receptor compartment, is there a general 'rule of thumb' that allows us to predict which SLC can be assessed *via* activation of a specific GPCR? We investigated whether an existing model could be used to explain the apparent potency shifts observed in the TRACT assays in this thesis and comparable assays from literature. In essence, the apparent potency shift of an agonist in the presence of an uptake process is the result of a discrepancy between the amount of substrate that is added to the cells and the actual substrate concentration at the receptor compartment due to the removal of the agonist. Two previously reported models describe the substrate concentration at the receptor compartment as a function of the added substrate concentration, the affinity of the substrate for the uptake process and a factor that represents the capacity or magnitude of the uptake process[51,52].

Before we discuss the two models, we should first describe the kinetics of a saturable uptake mechanism, of which the capacity/rate of uptake (V) is defined by the Michaelis-Menten equation:

$$V = \frac{V_{max} \times [S]_a}{[S]_a + K_m}$$

where $\mathbf{V_{max}}$ is the maximal capacity or rate of uptake at which the substrate can be transported in that system (usually in pmol/mg protein/min), $\mathbf{K_m}$ is the Michaelis-Menten constant, which is the concentration of substrate at which 50% of $V_{max}$ is achieved (sometimes referred to as substrate affinity or substrate activity), and $\mathbf{[S]_a}$ is the substrate concentration that was added to the medium. The ratio $V_{max}/K_m$ is often used to express the **transport efficiency** of the system and compares the uptake of multiple substrates in the same assay system and efficiency between different transporter systems. The higher the transport efficiency, the more volume of substrate is 'cleared' from the medium per time unit[45].

*8.4.1 – Langer & Trendelenburg model*

In 1969, Langer and Trendelenburg formulated a model which states that the presence of a saturable uptake process shifts the concentration-effect curve of a transported agonist if its affinity for the uptake process is in a similar range as its potency towards the receptor[51]. According to this model, the substrate concentration at the receptor compartment is described, after rearrangement of the original formula, as:

$$[S]_r = \frac{[S]_a^2 + \alpha K_m [S]_a}{[S]_a + K_m}$$

where $\mathbf{[S]_r}$ is the substrate concentration at the receptor compartment, $\mathbf{[S]_a}$ is the added substrate concentration, $\mathbf{K_m}$ is the Michaelis-Menten constant and $\boldsymbol{\alpha}$ is the maximal

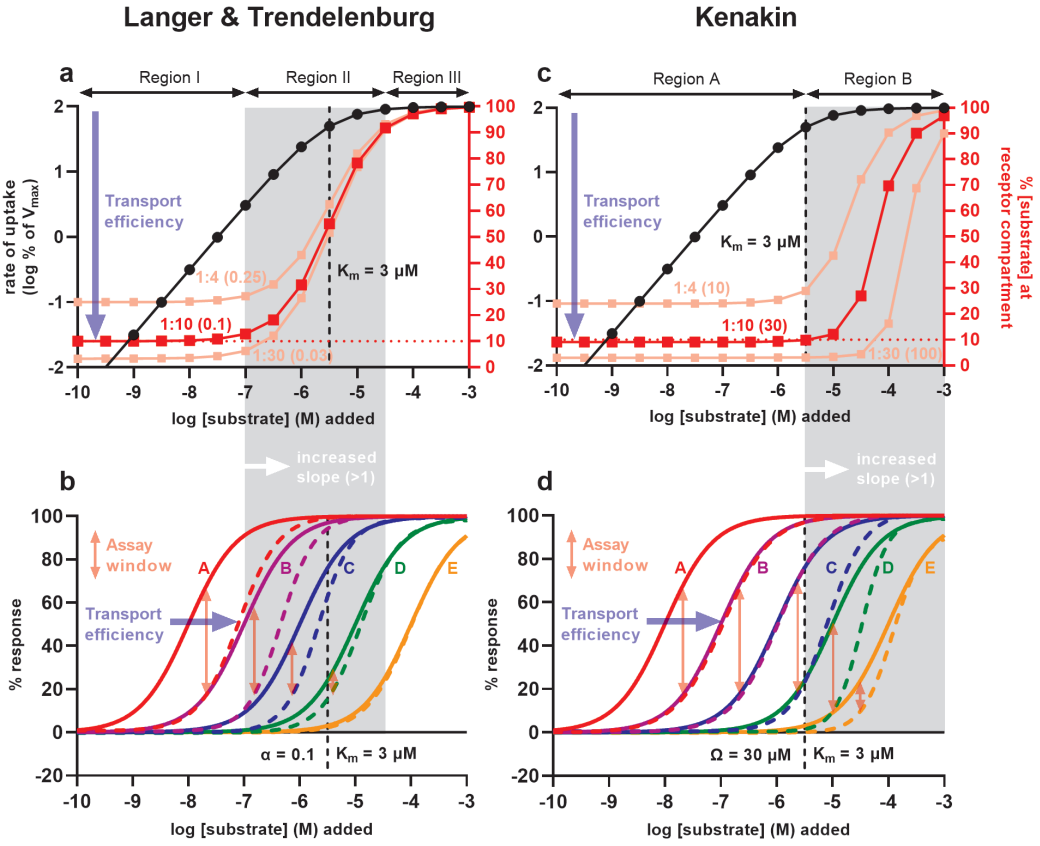


**Figure 8.2** – Two models describing the effect of a saturable uptake mechanism on the concentration and concentration-effect curves of G protein-coupled receptor (GPCR) agonists. (**a,b**) Model by Langer & Trendelenburg[51], (**c,d**) model by Kenakin[52]. (**a,c**) Simulated curves of the logarithmic rate of uptake (left y-axis, circles, 100% = $V_{max}$) and the relative substrate concentration at the receptor compartment ($[S]_r$, right y-axis, squares) plotted against the added substrate concentration ($[S]_a$). Rate of uptake is simulated using the Michaelis-Menten equation (log $K_m$ = –5.5). The relative $[S]_r$ is simulated using the equations of (**a**) Langer & Trendelenburg, or (**c**) Kenakin (log $K_m$ = –5.5), then shown as ($[S]_r/[S]_a$)x100%. The ratio along each curve signifies $[S]_r/[S]_a$ when $[S]_a << K_m$, with the value of (**a**) the maximal substrate fraction at the receptor compartment (α, unitless) or (**c**) the maximal capacity of the substrate removal process (Ω, in µM) in brackets. (**b,d**) Non-linear fits of simulated concentration-effect curves of five theoretical transported GPCR agonists (A–E) each with 10-fold difference in potency (log $EC_{50}$ = –8, –7, –6, –5, –4) and the same $K_m$, using the model of (**b**) Langer & Trendelenburg (**Figure 8.3i**, α = 0.1, log $K_m$ = –5.5, slope = 1), or (**d**) Kenakin (**Figure 8.4i**, log Ω = –4.5, log $K_m$ = –5.5, slope = 1). Solid and dashed curves describe agonist responses in the absence or presence of the uptake process, respectively. (**a,b**) In Region I, $[S]_a << K_m$ and the curve shift is proportional to the value of α; in Region II (grey area), $[S]_a$ nears $K_m$ and curves show increased slopes and diminished shifts as the $EC_{50}$ increases; in Region III, $[S]_a >> K_m$ and no curve shift is observed. (**c,d**) In Region A, $[S]_a < K_m$ and the curve shift is proportional to the value of Ω; in Region B (grey area), $[S]_a > K_m$ and curves show increased slopes, with the magnitude of the shift dependent on Ω. Transport efficiency (i.e., $V_{max}/K_m$) is related to α and Ω and indicates the maximal degree of curve shift. The assay window indicates the maximal difference between the agonist response ± uptake process. The graphical representation of the curves is based on Langer & Trendelenburg[51]. Data were simulated and visualized using GraphPad Prism v9.

hypothetical fraction of the added substrate that is present at the receptor compartment when $[S]_a << K_m$ (e.g., if 10% of added substrate is at the receptor compartment, then $\alpha = 0.1$) (**Figure 8.2a**). In the original article, the value of $\alpha$ was set at 0.1 and represented a 10-fold sensitization of the innervated tissue to norepinephrine in the presence of cocaine (i.e., uptake inhibition), although the authors stated that sensitizations up to 100-fold (i.e., $\alpha = 0.01$) were observed *in vivo*. Implicitly, $\alpha$ is dependent on the transport efficiency. $[S]_r$ can be introduced into the Hill equation – which describes the concentration-effect relationship of a receptor–agonist complex[53]:

$$\text{response} = \frac{\text{Bottom} + (\text{Top} - \text{Bottom})}{1 + 10^{(\log EC_{50} - \log[S]_r)n}}$$

where **Bottom** and **Top** indicate the minimal and maximal response, respectively, $\mathbf{EC_{50}}$ is the agonist potency (i.e., substrate concentration at which 50% of the maximal response is achieved) and **n** is the Hill coefficient defining the slope of the curve. In the presence of the uptake process, Langer and Trendelenburg define three substrate concentration regions in which the agonist response at the receptor is affected (**Figure 8.2a,b**):

- in **Region I**, when $[S]_a << K_m$ , the uptake rate is linear with the substrate concentration since the uptake rate becomes $V = (V_{max}/K_m)[S]_a$ and $[S]_r$ is at a constant fraction of $[S]_a$ (defined by $\alpha$). Here, the agonist curve shifts to the right with a magnitude dependent on $\alpha$ (e.g., $\alpha = 0.1$ indicates a 10-fold shift);

- in **Region II**, when $[S]_a \approx K_m$, uptake is gradually less linear and nears saturation, during which $[S]_r$ increases and gets closer to $[S]_a$. Here, two phenomena are expected to occur: 1) the rightward shift of the curves will diminish as the agonist potency ($EC_{50}$) increases, and 2) the slope of the curve will increase as $[S]_a$ approaches $K_m$;

- in **Region III**, when $[S]_a >> K_m$, the uptake rate equals $V_{max}$ and $[S]_r$ equals $[S]_a$. Here, no shift is observed as the agonist curve overlaps with the curve in the absence of uptake.

From this model, it is apparent that in Region I the agonist curve shift is dependent on the degree of transport efficiency. However, in Region II and III the transport efficiency is less important in determining $[S]_r$ and instead $[S]_r$ is driven by the $K_m$ of the agonist. This means that even with a low value for $\alpha$ (i.e., a high transport efficiency) the predicted curve shifts in these regions will not increase in magnitude, despite the larger transport capacity.

To determine whether the Langer & Trendelenburg model could be used to describe the TRACT assay data in this thesis, we simulated the models using the $EC_{50}$ and slope of the substrate response for the GPCR in the absence of uptake, the average $K_m$ that is reported for the respective SLC in **Appendix Table A.1** (as the $K_m$ was not determined in the current studies) and an arbitrary value for $\alpha$ of 0.01. The resulting simulated data points were fitted using non-linear regression with a variable slope (i.e., the Hill equation) and compared to fits that were directly derived from the substrate response curves ± SLC of TRACT assays in the chapters of this thesis (**Figure 8.3**). In addition, we compared the

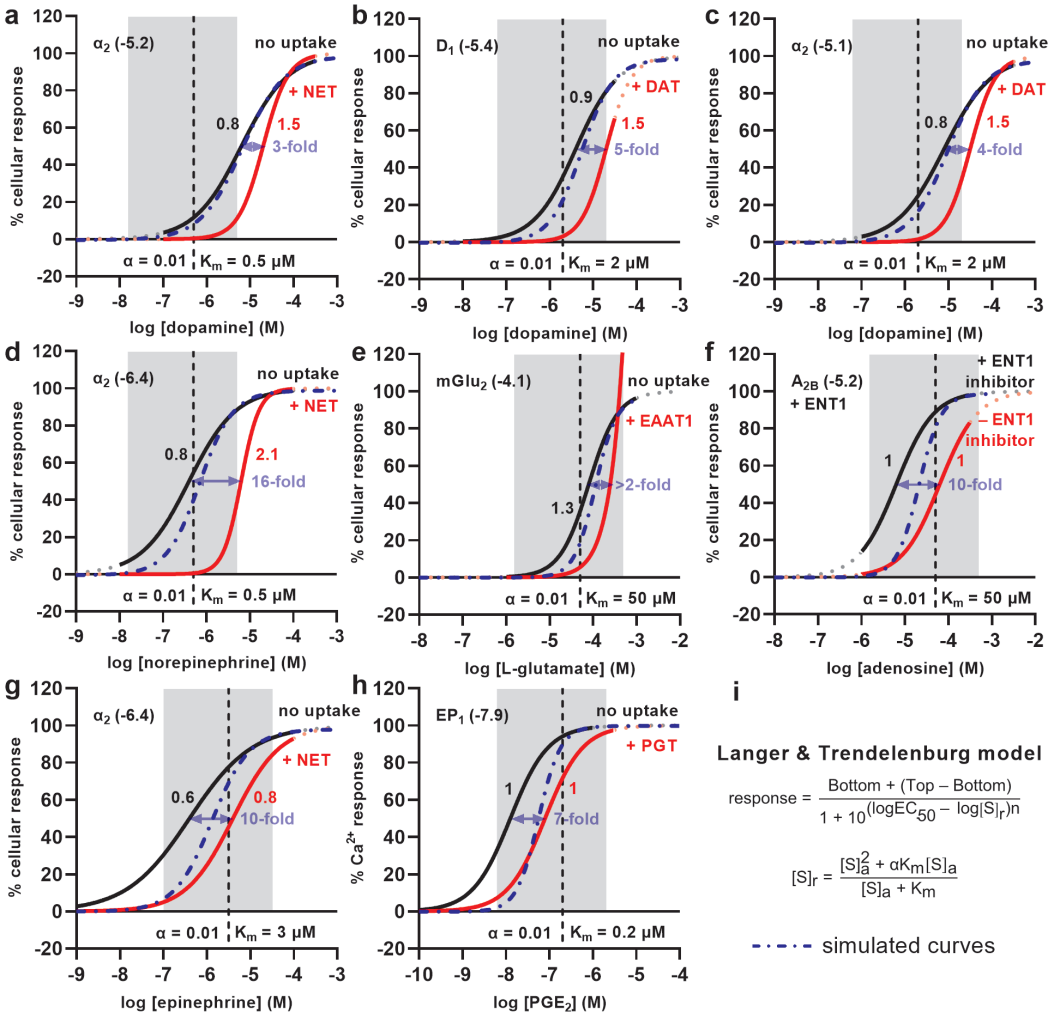


**Figure 8.3** – Non-linear fits of TRACT assays reported in this thesis or in literature and simulated concentration-response curve using the Langer & Trendelenburg model. The data is presented as the relative agonist-induced response on the GPCR in the absence (black solid curve) or presence (red dashed curve) of an SLC, which were generated using $EC_{50}$ values from the respective sources. Numbers next to the curves indicate the slope. The blue dashed curve is a simulation of the Langer & Trendelenburg model (**i**), using the log $EC_{50}$ (in M, stated next to the receptor subtype) and slope in the absence of uptake (n) from the source, the average $K_m$ reported in **Appendix Table A.1** for each substrate–SLC couple, and α = 0.01 (signifying a 100-fold maximal curve shift; further decreasing this value did not substantially the magnitude of the curve shift). Grey area indicates Region II of uptake (check **Figure 8.2a,b**). (**a**) Dopamine, alpha-2 adrenergic receptor ($\alpha_2$, log $EC_{50}$ = –5.2), norepinephrine transporter (NET, log $K_m$ = –6.3) (**Chapter 4**). (**b**) Dopamine, dopamine receptor D1 ($D_1$, log $EC_{50}$ = –5.4), dopamine transporter (DAT, log $K_m$ = –5.7) (**Chapter 3**). (**c**) Dopamine, $\alpha_2$ (log $EC_{50}$ = –5.1), DAT (log $K_m$ = –5.7) (**Chapter 3**). (**d**) Norepinephrine, $\alpha_2$ (log $EC_{50}$ = –6.4), NET (log $K_m$ = –6.3) (**Chapter 4**). (**e**) L-glutamate, metabotropic glutamate receptor 2 ($mGluR_2$, log $EC_{50}$ = –4.1), excitatory amino acid transporter 1 (EAAT1, log $K_m$ = –4.3) (**Chapter 6**). (**f**) Adenosine, adenosine $A_{2B}$ receptor ($A_{2B}$, + 1 μM dipyridamole (ENT1 inhibitor), log $EC_{50}$ = –5.2), equilibrative nucleoside transporter 1 (ENT1, log $K_m$ = –4.3) (Vlachodimou *et al.*)[23]. (**g**) Epinephrine, $\alpha_2$ (log $EC_{50}$ = –6.4), NET (log $K_m$ = –5.5) (**Chapter 4**). (**h**) $PGE_2$, prostaglandin receptor EP1 ($EP_1$, log $EC_{50}$ = –7.9), prostaglandin transporter (PGT, log $K_m$ = –6.7) (Chi *et al.*)[54]. Data were simulated and visualized using GraphPad Prism v9.

model to concentration-effect curves derived from two other publications: the label-free cellular response of adenosine on U2OS cells expressing $A_{2B}AR$ and ENT1 in the presence or absence of the ENT1 inhibitor dipyridamole (**Figure 8.3f**)[23], and the $Ca^{2+}$ response of prostaglandin $PGE_2$ on HEK293 cells expressing prostaglandin receptor $EP_1$ in the presence or absence of the prostaglandin transporter (PGT, SLCO1A2) (**Figure 8.3h**)[54].

In **Figure 8.3**, the black curve indicates the substrate-induced cellular response in the absence or inhibition of uptake, whereas the rightward-shifted red curve is the cellular response in the presence of the uptake process. In the absence of uptake, the $EC_{50}$ value (the concentration needed for half-maximal effect) for all substrates lies within Region II or III of the uptake process, which depends on the $K_m$ of the substrate. When imposing the simulated curves from the model (**Figure 8.3i**) into each respective graph (blue dashed curves), it is evident that the model is unable to completely describe the rightward shift of the response curve in the presence of uptake – i.e., the simulated curves do not overlap with the actual data (red curves). For example, the rightward shift of the norepinephrine response in the presence of NET is 16-fold compared to cells lacking NET, whereas the simulated curve only predicts a fraction of this shift (**Figure 8.3d**). When the $EC_{50}$ nears Region I, as is the case with $PGE_2$ (**Figure 8.3h**), the simulated curve is closer to the response in the absence of uptake, although the slope of this curve is not in line with the actual data. Increasing the 'transport efficiency' in the model (i.e., $\alpha \rightarrow 0$) did not result in a larger rightward shift of the predicted response curve, which indicates there is a limit to this model and it does not accurately describe the observed curve shifts of the TRACT assay.

*8.4.2 – Kenakin model*

A second model was postulated by Kenakin in his book 'A Pharmacology Primer', in which he describes a saturable adsorption site that acts as a sink claiming a portion of the ligand added to the medium[52]. Foremost, this adsorption site refers to any surface in an *in vitro* experiment (e.g., the plastic of a cell culture plate) to which the ligand under investigation can bind, leading to a reduction of the free concentration and an overestimation of the true concentration (and, thus, potency) of the ligand at the receptor compartment. More generally, this model can describe any process that reduces the free ligand concentration, such as enzymatic degradation or uptake of the ligand. Thus, Kenakin defines the free ligand concentration ($[S]_r$) as the total ligand concentration ($[S]_a$) minus the ligand concentration at the adsorption site, which can be described according to the mass action equation and results in the following quadratic formula:

$$[S]_r = [S]_a - \frac{1}{2}\left([S]_a + K_m + \Omega - \sqrt{([S]_a + K_m + \Omega)^2 - 4[S]_a\Omega}\right)$$

where $\mathbf{[S]_r}$ is the substrate concentration at the receptor compartment, $\mathbf{[S]_a}$ is the added substrate concentration, $\mathbf{K_m}$ is the Michaelis-Menten constant (defined in the original model as the equilibrium dissociation constant of the ligand at the adsorption site) and $\mathbf{\Omega}$ is the maximal capacity of the substrate removal process (defined in the original model as the maximal number of adsorption sites) (**Figure 8.2c**). It should be noted that all four

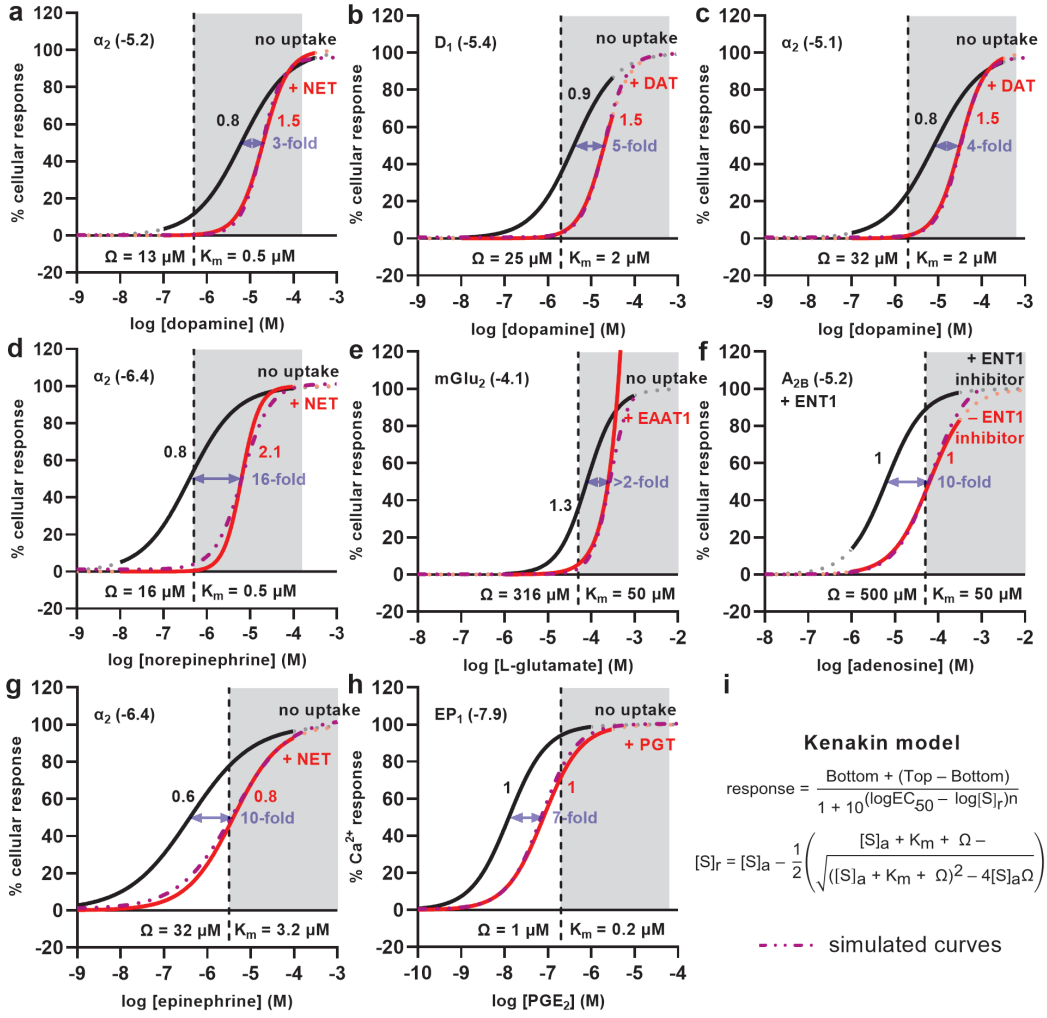


**Figure 8.4** – Non-linear fits of TRACT assays in this thesis or in literature and simulated concentration-response curve using the Kenakin model. The data is presented as the relative agonist-induced response on the GPCR in the absence (black solid curve) or presence (red dashed curve) of an SLC, which were generated using $EC_{50}$ values from the respective sources and are identical to **Figure 8.3**. Numbers next to the curves indicate the slope. The purple dashed curve is a simulation of the Kenakin model (**i**), using the log $EC_{50}$ (in M, stated next to the receptor subtype) and slope in the absence of uptake (n) from the source, the average $K_m$ reported in **Appendix Table A.1** for each substrate–SLC couple, and a manually selected value for Ω (by trial-and-error) that caused the simulation to overlap with the red curve. Grey area indicates Region B of uptake (check **Figure 8.2c,d**). (**a**) Dopamine, alpha-2 adrenergic receptor ($\alpha_2$, log $EC_{50}$ = –5.2), norepinephrine transporter (NET, log $K_m$ = –6.3), log Ω = –4.9 (**Chapter 4**). (**b**) Dopamine, dopamine receptor D1 ($D_1$, log $EC_{50}$ = –5.4), dopamine transporter (DAT, log $K_m$ = –5.7), log Ω = –4.6 (**Chapter 3**). (**c**) Dopamine, $\alpha_2$ (log $EC_{50}$ = –5.1), DAT (log $K_m$ = –5.7), log Ω = –4.5 (**Chapter 3**). (**d**) Norepinephrine, $\alpha_2$ (log $EC_{50}$ = –6.4), NET (log $K_m$ = –6.3), log Ω = –4.8 (**Chapter 4**). (**e**) L-glutamate, metabotropic glutamate receptor 2 ($mGluR_2$, log $EC_{50}$ = –4.1), excitatory amino acid transporter 1 (EAAT1, log $K_m$ = –4.3), log Ω = –3.5 (**Chapter 6**). (**f**) Adenosine, adenosine $A_{2B}$ receptor ($A_{2B}$, + 1 µM dipyridamole (ENT1 inhibitor), log $EC_{50}$ = –5.2), equilibrative nucleoside transporter 1 (ENT1, log $K_m$ = –4.3), log Ω = –3.3 (Vlachodimou *et al.*)[23]. (**g**) Epinephrine, $\alpha_2$ (log $EC_{50}$ = –6.4), NET (log $K_m$ = –5.5), log Ω = –4.5 (**Chapter 4**). (**h**) $PGE_2$, prostaglandin receptor EP1 ($EP_1$, log $EC_{50}$ = –7.9), prostaglandin transporter (PGT, log $K_m$ = –6.7), log Ω = –6.0 (Chi *et al.*)[54]. Data were simulated and visualized using GraphPad Prism v9.

parameters are in the same unit of concentration (i.e., μM), indicating that Ω cannot be substituted for the maximal transport capacity ($V_{max}$) of the uptake process. The actual value of Ω comprises various aspects and takes into account the $V_{max}$, but also other factors such as the diffusion rate of the substrate into and from the receptor compartment. When $[S]_r$ is introduced into the Hill equation, similar to the Langer & Trendelenburg model, we can define two major substrate concentration regions in which the agonist response at the receptor is affected (**Figure 8.2c,d**):

- in **Region A**, when $[S]_a \leq K_m$ , the uptake rate is either linear with the substrate concentration ($V = (V_{max}/K_m)[S]_a$ when $[S]_a << K_m$) or becomes gradually less linear as $[S]_a$ approaches $K_m$. In this region, $[S]_r$ is at a constant fraction of $[S]_a$ and the agonist curve shifts to the right with a magnitude dependent on the ratio between Ω and $K_m$;

- in **Region B**, when $[S]_a \geq K_m$, the uptake rate gradually nears saturation, during which $[S]_r$ increases and gets closer to $[S]_a$. Here, two phenomena are expected to occur when Ω remains constant: 1) the rightward shift of the curves will diminish as the agonist potency ($EC_{50}$) increases, and 2) the slope of the curve will increase as $[S]_r \rightarrow [S]_a$. The end of Region A and start of Region B lie to the left when Ω decreases, and to the right when Ω increases;

In this model, the magnitude of the shift of the concentration-response curves is dependent on the transport efficiency (i.e., $V_{max}/K_m$) at all substrate concentrations, in contrast to the Langer & Trendelenburg model where only the curve shift in Region I was mainly governed by the transport efficiency. This means that in Region B, even when $[S]_a >> K_m$, a curve shift and slope change may be observed when the value for Ω is sufficiently large.

The Kenakin model was used to describe the TRACT assay data in this thesis and other publications by simulation of concentration-response curves using the same $EC_{50}$, slope and $K_m$ for the substrate as in **Figure 8.3**. The value for Ω was manually selected for each simulation based on the coordinates of the final curve in relation to the real data (i.e., when both curves overlap) (**Figure 8.4**). The black and red curves (i.e., substrate-induced cellular response in the absence or presence of uptake, respectively) in **Figure 8.4** are identical to **Figure 8.3**. When imposing the simulated curves from the model (**Figure 8.4i**) into each respective graph (purple dashed curves), we observe that the model is able to describe both the rightward shift as well as the change in slope of the response curve for all TRACT assays – i.e., the simulated curves overlap with the actual data (red curves). For example, the response curves for dopamine and norepinephrine on $\alpha_2$R in the presence of NET have increased slopes, whereas the slope is not substantially increased for epinephrine (**Figure 8.4a,d,g**). According to the model, the shallow curve of epinephrine could be explained by the higher values for $K_m$ and Ω, resulting in a parallel curve shift in Region A. Indeed, it is expected that dopamine and norepinephrine have lower $K_m$ values than epinephrine, but the latter two substrates should have equal $V_{max}$ values[55]. Moreover, it is evident that a higher $K_m$ value of a substrate for an SLC (e.g., L-glutamate, adenosine) requires a higher value for Ω to accompany the removal of sufficient substrate quantities in order to explain

the observed curve shifts (**Figure 8.4e,f**). It should be noted that number of variables in the Trendelenburg and Kenakin models are equal, with the only differences being the α/Ω factors and the form of the $[S]_r$ equations. Tuning the value of Ω had a profound effect on the shift and slope of the resulting simulated curve, whereas a limit was reached for these properties in the simulation with the Trendelenburg model when the value of α was further reduced. Although this may denote Ω as a 'fudge factor', here it illustrates that the observed curve shifts are dependent on both the substrate $K_m$ and the $V_{max}$. Altogether, the Kenakin simulations illustrate that the TRACT assay should work for any SLC for which the substrate capacity, and thus the transport efficiency, is high enough in relation to the potency of that substrate on the GPCR. Since most SLCs have no reported transport efficiencies, we advise to select a GPCR for which the substrate $EC_{50}$ is lower than 30 × the substrate $K_m$ for the SLC (see **Appendix Table A.1** for an overview of substrate affinity and potency values).

## 8.5 – Factors of influence in the TRACT assay

It is challenging to predict upfront whether a specific SLC–GPCR pair is amenable to assessment in the TRACT assay. Although the Kenakin model is able to describe the agonist response curve shifts that were observed in TRACT assays, there are factors and limitations to the substrate, SLC and GPCR that should be considered when selecting any SLC–GPCR pair for assessment (**Figure 8.5**).

The $K_m$ of a substrate is a constant for a specific SLC and generally varies less across experiments, although it may be slightly higher in heterologous expression systems versus native tissue. For example, the $K_m$ of dopamine for DAT (various species) is 0.03–0.5 μM in the brain compared to 0.1–5 μM in cells overexpressing DAT[56]. In contrast, the $V_{max}$ is considerably more prone to variation, as it is dependent on the turnover number – $k_{cat}$, also known as the turnover rate, which is the number of complete transport cycles a transporter makes on average per unit of time[57] – and the total number of transporters expressed on the cell ($[E_T]$), according to:

$$V_{max} = k_{cat} \times [E_T]$$

Within one cellular system, the $[E_T]$ is more or less constant for all substrates. However, the transporter density can vary greatly between endogenous cell lines and heterologous (over) expression systems, which can result in widely different $V_{max}$ values between experiments. For example, the $V_{max}$ of dopamine for DAT was shown to range between 0.004–1925 pmol/min/mg protein depending on the DAT species and cell line origin[56]. In this thesis, $K_m$ and $V_{max}$ values were not determined for the respective SLC cell lines, thus no definitive conclusions can be drawn regarding the contribution of $V_{max}$ to the value of Ω and the optimal transport efficiency. Future investigations would certainly benefit from such kinetic characterizations, which could aid in the development of better predictive models and assays. For instance, if we know which value of $V_{max}$ corresponds to the value of Ω, we could predict the agonist curve shift of a substrate using the Kenakin model and $V_{max}/K_m$ values that were measured in-house.

$V_{max}$ is influenced by both $k_{cat}$ and $[E_T]$. The $k_{cat}$ is specific to the substrate and defines the sum of multiple micro-rate constants that characterize a transport cycle, including substrate association to ($k_{on}$) and dissociation from ($k_{off}$) the transporter, binding of co-substrate(s), the conformational change of the transporter from an outward- to an inward-facing position, the unbinding of the (co-)substrate(s) from the transporter, and the relocation of the transporter from an inward-facing to an substrate-accessible outward-facing conformation (**Figure 8.5**)[58,59]. Hence, the $k_{cat}$ is influenced by factors such as the type of substrate, concentration gradients of co-substrates (e.g., ions), membrane potential, temperature, post-translational modifications to the transporter and the presence of regulatory proteins[57,60]. The true value of $k_{cat}$ is difficult to determine *in vitro* and is often inaccessible, although significant advancements have been made to predict micro-rate constants using systems biology simulations[58,61,62]. In general, for ion channels – which allow free but selective diffusion of ions – the turnover number is in the range of $10^7$–$10^9$ $s^{-1}$, whereas SLC transporters have much slower rates ($10^{-1}$–$10^3$ $s^{-1}$) which often makes it difficult to detect transporter-mediated currents for large-scale electrophysiological assessments[61]. For example, the turnover of neurotransmitters by NET, DAT and SERT is relatively slow (0.1–2 $s^{-1}$)[63–66], nucleoside transport by ENT1 is 100-fold faster (200 $s^{-1}$)[67] and turnover of glutamate by EAATs is highly dependent on the subtype (EAAT1, 16 $s^{-1}$; EAAT2, 14–41 $s^{-1}$, EAAT3, 90–110 $s^{-1}$; EAAT4, <3 $s^{-1}$; EAAT5, <1 $s^{-1}$)[68]. Thus, transporters with a slow $k_{cat}$ would require a relatively higher $[E_T]$ to attain a comparable $V_{max}$.

As the $k_{cat}$ is a constant for each substrate, manipulation of the $[E_T]$ (e.g., *via* overexpression of the transporter) is experimentally the most straightforward method to change the $V_{max}$ and increase the specific signal-to-noise ratio of an uptake system (**Figure 8.5**). However, there is a physical limit to the amount of membrane proteins a cell can harbor at any moment, which can pose constraints on the maximal value of $V_{max}$ for any SLC in a specific cell type[62,69]. For example, Belo do Nascimento *et al.* have demonstrated that the maximal uptake rate of glutamate in a HEK293 cell line with inducible expression of EAAT2 – i.e., the same JumpIn system as the cells in this thesis – does not increase linearly with increased EAAT2 expression, but rather shows saturation of the uptake capacity ($V_{max}$) at higher levels of the transporter in addition to a slightly increased $K_m$ value[70]. In addition, higher transporter levels resulted in a decreased apparent potency of the EAAT2 inhibitor WAY-213,613, which was attributed to an increased number of binding sites. Similar observations were made for the serotonin (SERT, SLC6A4)[71] and dopamine (DAT, SLC6A3)[72] transporters, suggesting that alterations of ligand potency as a result of limiting transporter density might be common for most transporters. Altogether, this may indicate that not all transporters of the total transporter pool at the cell membrane are contributing to the maximal uptake activity, which could indicate a 'transporter reserve' analogous to the 'receptor reserve' concept that applies to GPCRs (**Figure 8.5**) – i.e., the occupancy of only a small fraction of the total receptors is required to produce the maximal functional response[52]. Interestingly, in the TRACT assays for DAT and NET (**Chapter 3 and 4**), as well as the phenotypic assay for EAAT1 (**Chapter 6**), we observed that inhibitory potency ($IC_{50}$) values of the respective SLC inhibitors were in general up to 10-fold higher compared to literature values. One cause of this may be that higher competing concentrations of

substrate were used in the TRACT assay compared to conventional assays (e.g., radioligand uptake), which could lead to increased competition with the SLC inhibitor and a rightward shift in potency. An additional explanation might be the presence of a transporter reserve in these inducible overexpression cell lines that could alter transporter kinetics and result in a slight underestimation of the true inhibitory potency. This should be considered when the TRACT assay is employed for pharmacological characterizations.

In a typical *in vitro* experiment, the volume of the extracellular compartment (i.e., the culture medium or buffer) – 100 µl in our TRACT assays – is large compared to the accessible monolayer of cells that are attached at the bottom of the microtiter plates. In the absence of a saturable uptake process, the substrate can freely diffuse to the cell membrane resulting in an equal concentration at the cell surface and in the bulk solution of the extracellular compartment. However, there is a thin unstirred water layer (µm range) coating adherent cell monolayers where free diffusion of substrate is slower than in 'stirred' bodies of water[52,73,74]. In essence, this unstirred layer is directly accessible to the cell membrane and can be compared to the receptor compartment or 'biophase' (**Figure 8.5**). Especially in 96- or 384-well culture formats, this layer is larger than in perfused tissues as it is not possible to stir or constantly homogenize the extracellular medium. If there is a process that removes the substrate from this unstirred water layer, e.g., uptake *via* an SLC, then the substrate concentration in this layer depends on the uptake rate and the diffusion rate of the substrate from the bulk solution to the unstirred water layer[75]. The substrate concentration in this layer will be lower than the bulk solution as long as the uptake is not saturated, even

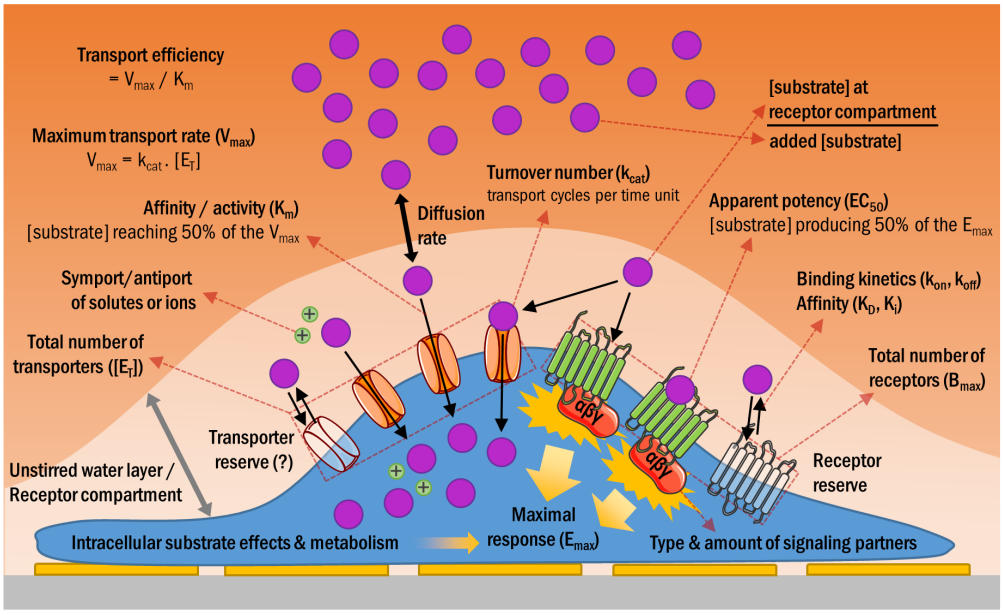


**Figure 8.5** – Factors that influence the substrate-induced cellular response on cells expressing GPCRs and/or SLCs for that substrate.

in the presence of a vast excess of substrate in the bulk solution. Thus, the presence of the unstirred water layer in a microtiter format may in part explain the magnitudes of the agonist curve shifts in TRACT assays.

The readout of a TRACT assay is constituted by the activation of a GPCR by the SLC substrate, which leads to recruitment of signaling partners and subsequent changes in cell morphology that are measured as a change in impedance[76]. As is evident from the Langer & Trendelenburg and Kenakin models described in the previous section, the apparent potency ($EC_{50}$) of the substrate on the GPCR – in relation to the $K_m$ and capacity of the SLC – determines the extent of the response curve shift in the presence of the SLC. In general, if the SLC transport efficiency is sufficient, a higher substrate potency (i.e., lower $EC_{50}$ value) results in a larger curve shift (**Figure 8.2b,d**). There are several factors that can influence the $EC_{50}$ of a substrate towards a receptor (**Figure 8.5**). The total number of receptors ($B_{max}$) on a cell can affect the maximal response ($E_{max}$) and $EC_{50}$, as higher receptor densities increase the $E_{max}$ and enhance the ligand potency[52]. The receptor density, just like the total number of transporters ($[E_T]$), is the most straightforward to control experimentally by using recombinant expression systems, which we used in **Chapter 6** for the transient expression of $mGluR_2$. It should be noted that the maximal receptor-mediated response of a substrate is limited by the availability, subtype and kinetics of intracellular signaling partners (i.e., G proteins, β-arrestins, etc.), as there is a finite number of signal amplification reactions that can occur within each cell per time unit[13,77]. Moreover, more comprehensive GPCR concepts, such as receptor desensitization, internalization, allosteric modulation and biased agonism could all have a profound effect on the substrate $EC_{50}$ in an impedance-based assay[78,79]. Thus, selecting the appropriate GPCR to generate a cellular response is crucial when setting up a TRACT assay.

### 8.6 – GPCR-independent phenotypic SLC assays using impedance

In essence, the xCELLigence provides a phenotypic readout of a cell's function, as it is able to capture any change in cellular properties upon perturbation with a ligand; the 'phenotype' that is observed (i.e., a characteristic increase or decrease of impedance) depends on which pathway is triggered. Besides GPCR-mediated contributions to the cellular response, there may be receptor-independent mechanisms that have an effect on the magnitude of the overall response in the presence of an SLC.

In **Chapter 6 and 7**, we observed that in JumpIn cells overexpressing EAAT1 – but not $mGluR_2$ – the addition of glutamate or aspartate results in a strong increase of the Cell Index that peaked after two hours, which was at least six-fold greater in amplitude compared to rapid (15 min) $mGluR_2$-mediated responses. These responses were completely mediated by EAAT1, as both EAAT1 inhibitors UCPH-101 and TFB-TBOA inhibited the response of 1 mM glutamate/aspartate in a concentration-dependent manner. Since no GPCR was involved in this part of the response, we investigated the putative mechanism behind the EAAT1-mediated cellular response by live-cell imaging and targeted metabolomics. In actin-GFP-tagged cells, upon addition of glutamate JumpIn-EAAT1 cells started to spread on the

culture plate surface, which provides a visual explanation for the drastically increased Cell Index on xCELLigence. Glutamate uptake has previously been shown to induce cell swelling, as glutamate enters the cell with 3 $Na^+$ and 1 $H^+$ in exchange for 1 $K^+$ which increases the cell's osmolarity causing an influx of water[80–82]. This rapid uptake and increased cell volume may elicit intracellular $Ca^{2+}$ elevations, ATP release and autocrine receptor activation, which results in the formation of protrusions at the cell's edges, effectively altering the cell morphology[83,84]. The involvement of a cell swelling process in the EAAT1 cellular response was confirmed by reduced levels of intracellular taurine (i.e., an osmolyte that is released from the cell upon cell volume changes[85]) and inhibition of the response by ouabain (i.e., an inhibitor of $Na^+/K^+$-ATPase, which restores the $Na^+$ gradient and is crucial for glutamate uptake[86]). The glutamate-induced cellular response was highly reproducible and robust, as reflected by an excellent Z' factor of 0.85, which indicates that this assay can be used to screen for EAAT1 inhibitors. Moreover, these results demonstrate that SLC function can be assessed in a phenotypic assay in the absence of a substrate-activated GPCR.

## 8.7 – Application of impedance-based assays in SLC drug discovery: computational methods and compound screening

The use of computational techniques based on machine learning to design, generate and predict biological activity of new molecules for drug targets has increased in recent years[87–89]. Computer-aided drug design for SLCs has been mostly aimed at ligand-based approaches such as quantitative structure-activity relationship (QSAR) or pharmacophore modeling[90]. However, as a result of the increasing number of SLC crystal structures in the last ten years, structure-based methods such as ligand docking, free energy perturbations and molecular dynamics (MD) simulations are also aiding the rational design of SLC targeting drugs[91]. Nevertheless, in the absence of structural information ligand-based models can be highly informative and new models are being developed to speed up the drug discovery process. For example, proteochemometric (PCM) modeling can be seen as an extension of the more conventional QSAR studies, and has been successfully used to design novel, selective compounds based on molecular descriptors that describe the similarity between ligands and the target protein[1,92]. So far, PCM models have been used to accurately predict clinically relevant drug–transporter interactions[93] as well as the activity of inhibitors for organic anion transporting polypeptide 1B1 and 1B3 (OATP1B1/3, SLCO1B1/3)[94] and the sodium-glucose cotransporter 2 (SGLT2, SLC5A2)[2].

In **Chapter 5** we used a PCM model to perform virtual screening of a large database of synthesizable compounds (~700 million structures) to identify novel inhibitors of NET. Although several studies employed structure-based drug design – based on homology models of human SERT or *Drosophila* DAT – for the identification of prescription drugs or novel molecules that inhibit NET[27,95], this is the first time a large database is screened for NET using a PCM model. Using the model, which was trained on reported NET interaction data from the ChEMBL database, over 22,000 compounds were predicted to be active at NET. After similarity filtering, 32 of these compounds were synthesized and

screened at 10 μM in the TRACT assay that was described in **Chapter 4**. Interestingly, five of these compounds, which were structurally diverse, were identified as hits, with inhibitory potencies in the mid-to-low nanomolar range. The chemical space around one of these hits is currently being investigated in our lab, which might lead to the discovery of novel, potent NET inhibitors with distinct pharmacological properties. On the one hand, this study demonstrates the power of identifying new active molecular scaffolds with PCM modeling, which could become a more common approach in computer-aided drug design for SLCs. On the other hand, we demonstrate the screening potential of the TRACT assay, which shows that this assay could be used for primary and follow-up screens in SLC drug discovery programs.

### 8.8 – Application of impedance-based assays in SLC drug discovery: functional assessment of genetic variants

Proper functioning of SLCs is key to maintain homeostasis and warrant cell signaling. Mutations in SLC genes, causing either a loss- or gain-of-function, have been associated with faltering drug efficacy, distribution and toxicity, in addition to population-specific monogenic (inheritable) diseases[96,97]. Genetic variability of SLCs is common in humans, as it is estimated that each individual genome contains 30 SLC variants that alter the transporter function[96]. Functional characterization of SLC variants is important as it aids the association of disease phenotype with genotype, which could be the basis for the design of new therapeutic strategies. A notable example is the development and approval of sodium-glucose cotransporter 2 (SGLT2, SLC5A2) inhibitors (i.e., gliflozins) for the treatment of hyperglycemia in type 2 diabetes patients, as mutations in the SLC5A2 gene were initially associated with familial renal glucosuria[98]. Other metabolic disorders, such as non-alcoholic fatty liver disease, obesity and insulin resistance are linked to polymorphisms in UCP1 (SLC25A7), NaCT (SLC13A5) and MCT11 (SLC16A11)[99]. Although the clinical tyrosine kinase inhibitor linifanib has been identified as a potent UCP1 inducer – reactivating thermogenesis, for the potential treatment of obesity[100] –, there are no specific compounds yet that target these transporters, providing an immense opportunity for drug discovery. Over the last two decades, another major class of SLCs, the neurotransmitter transporters, has been largely associated with missense mutations that cause functional deficits and protein misfolding, which implicates transporters with various neurological diseases such as ataxia, Parkinson's disease, epilepsy and mental disorders[101]. The main hurdle towards a basic understanding of the clinical consequences of these genetic SLC variants has been the shortage of functional studies, which was mostly hampered by the lack of proper assay platforms or the absence of structural information of the protein. Thus, with the rapid increase in the number of crystal and cryo-EM structures of human SLCs[102–104], as well as the development of novel functional assays[105] – such as the ones described in this thesis – we are more than ever equipped with the right tools to characterize and mechanistically interpret SLC variants in the light of disease and drug discovery.

As another demonstration of the versatility of cell-based label-free assays, we employed the xCELLigence to investigate the functional consequences of SLC variants. We selected EAAT1 (SLC1A3) as a model transporter since we had already developed an assay for this transporter (**Chapter 6**) and disease-related mutants had been reported in literature. SLC1A3 variants have been associated with the etiology of very rare cases of episodic ataxia type 6 (EA6), which has been functionally attributed to altered chloride conductivity and/or glutamate transport[106]. In **Chapter 7**, we identified several missense mutations of SLC1A3 in cancer patients from the Genomic Data Commons (GDC) database of the National Cancer Institute. Since 3D structures of human EAAT1 – bound to $Na^+$ ions, substrates and/or inhibitors – are available[107,108], we rationally selected eight mutants from the GDC database based on their proximity to substrate and/or inhibitor binding sites, in addition to two EA6-related mutants (M128R, T318A) that had been reported to lose or retain glutamate transport function[106]. Using the functional assay from **Chapter 6**, we were able to measure glutamate- and aspartate-induced cellular responses, as well as inhibitory potencies of TFB-TBOA and UCPH-101 for all mutants. Mutants showed diverse substrate responses, either a decrease in the maximal response or alteration in the substrate potency. Interestingly, while most mutants showed reduced or unaltered inhibitory potency of the EAAT1 inhibitors, two mutants (A446E, L448Q) enhanced the $IC_{50}$ of both TFB-TBOA and UCPH-101. Ongoing experiments using MD simulations – which have previously been used to characterize $K^+$ coupling, the $Cl^-$ permeation pathway and M128R mutation of EAAT1[109–111] – could provide an additional substantiation of the *in vitro* data by investigating the conformational changes of mutant EAAT1 subdomains. These results demonstrate that xCELLigence can be used to functionally assess EAAT1 mutants, which could prove exemplary for other SLC variants that may be investigated on this platform in the future.

### 8.9 – Future perspectives – Label-free assays and opportunities for SLC drug discovery: where to next?

The ultimate purpose of any *in vitro* assay is to measure the activity of a molecule towards its intended target, which is exactly the rationale in early drug discovery: finding the right drug, for the right target, ideally as time- and cost-effectively as possible. The advantage of cell-based assays, as compared to purified protein or membrane fractions, is that activation or inhibition of the target of interest occurs in an environment that more closely mimics that of the cells *in vivo*[5]. The use of label-free assays, as opposed to assays based on radioactivity or fluorescence, may reduce the occurrence of artefacts and facilitates a more 'physiologically relevant' environment of the cell[9]. Phenotypic assays can be used as an 'unbiased' approach to find molecules with a desired biological effect, and by integration of phenotypic methods with target-based approaches (e.g., cells overexpressing the target of interest) the outcome can help understand complex mechanisms of action that may be more predictive of the clinical outcome of a drug treatment[112]. Thus, with a cellular background that is appropriate for the research question or the disease under investigation, label-free phenotypic assays can inform on both the potency of a molecule and its potential adverse effects[8,113]. This may lead to an overall better prediction of a molecule's *in vivo* efficacy and reduce the chance

of clinical failure of drug candidates, as poor efficacy is still a major cause of failed clinical trials and drug attrition[114]. The cell-based, label-free, impedance-based phenotypic assays that are described in this thesis are an attractive alternative to traditional SLC assays (see **Table 1.1, Chapter 1**) and may be implemented in drug discovery programs in the years to come.

The use of label-free impedance-based platforms in pharmacological research and life sciences in general has increased over the last few years. Besides their common use to monitor cell proliferation and viability[115], the applications of these technologies extend well beyond cell-based functional assays for GPCRs and SLCs. xCELLigence Cardio systems are routinely used to test the effect of compounds on cardiac contractility in (induced pluripotent stem cell-derived) cardiomyocytes, which offers fast, high-throughput screening of cardiotoxicity for drug safety assessment[116]. Moreover, real-time cell analysis is increasingly used as a platform to measure T cell-mediated killing of adherent cells[117] and has become the most common method to evaluate cytotoxicity of chimeric antigen receptor (CAR)-T cells, a highly promising immunotherapy for solid tumors[118,119]. In the wake of the recent COVID-19 pandemic, the xCELLigence has been used for rapid (<5 min) detection of severe acute respiratory syndrome coronavirus 2 (SARS-CoV-2) antibodies in serum samples on spike protein-coated E-plates, demonstrating the applicability of impedance measurements with cell-free approaches[120]. Although the possibilities with impedance-based biosensors are broad, a potential concern is that they offer a 'black box' readout, which would indicate that the mechanism by which a compound elicits a cellular response is unclear judging from the impedance changes alone[12]. However, just as with other functional assays a conventional solution to address this concern is to use appropriate controls, such as cell lines with and without the target of interest, the use of orthogonal assays, receptor antagonists or pathway-specific inhibitors (as shown in **Chapter 3, 4 and 6**) to deconvolute the signal and attribute parts of the response that are of interest to the research question. Thus, since impedance measurements can be used to detect a wide range of cellular behavior and are not limited to assessment of a single pathway, it is expected that versatile platforms such as xCELLigence will be implemented more often in biochemical studies.

In this thesis, we have focused on seven SLCs (DAT, NET and EAAT1/2/3/4/5) for the development of label-free impedance-based assays, of which three were assessed in a TRACT assay. However, there are many SLCs that transport a substrate that is also a GPCR ligand, which we have summarized in **Appendix Table A.1**. Besides providing an extensive overview of affinity and potency values for substrates on SLCs and GPCRs, this list may aid in the selection of SLCs for future TRACT assessment on xCELLigence; several of these – monocarboxylate transporters SMCT1/2 (SLC5A8/12), prostaglandin transporter PGT (SLCO2A1) and monoamine transporter PMAT (SLC29A4) – are subject to ongoing investigations in-house. It should be noted that the current list focuses on *human* SLCs and GPCRs, thus it does not include isoforms that are exclusively expressed in other mammals. Evidently, we did not report orphan SLCs and GPCRs (i.e., substrate is unknown). Since ~30% of SLCs and ~15% of GPCRs are considered orphan (**Chapter 2**), there may be additions to **Table A.1** in the future when these transporters and receptors are deorphanized. Even though vesicular transporters are included, we did not mention

mitochondrial transporters from the SLC25 family. Moreover, we have limited the overview to reported endogenous substrates that engage with both the SLC and GPCR, indicating that we exclude putative substrates (e.g., from large metabolic screens), substrates that *inhibit* SLCs or GPCRs, metabolic precursors of GPCR ligands (e.g., choline as a precursor of acetylcholine), non-GPCR ligands (e.g., taurine, glucose) and drugs/xenobiotics that share an SLC–GPCR pair. In line with this, we did not report substrates for other types of receptors (e.g., ligand-gated ion channels, nuclear receptors) that might result in cellular responses upon activation. Although in this thesis we emphasize TRACT assays based on modulation of GPCRs by *influx* of substrate by SLCs at the plasma membrane, there may be other possible assay set-ups to investigate SLCs with different modes of action and localizations. For example, sphingosine-1-phosphate (S1P) efflux *via* MFSD2B (SLC59A2) could be detected by applying the supernatant of the MFSD2B-expressing cells to a cell line expressing the S1P3 receptor and measuring the calcium response, as was described in a recent RESOLUTE-curated review[105]. Such a set-up could potentially be mimicked on an xCELLigence E-plate, for example by co-culturing cells that express either the SLC or GPCR. Alternatively, vesicular loading and subsequent release of neurotransmitters (e.g., monoamines, ATP) *via* $Ca^{2+}$-induced exocytosis of vesicles[121] may be detected in a similar manner, by using a substrate-'producing' cell line and a substrate-'responsive' cell line, although this has yet to be verified experimentally. Taken together, judging from the breadth of SLCs that are involved in the translocation of GPCR ligands, there is ample opportunity for TRACT assay development.

The advantage of impedance-based measurements is that they can capture any phenotypic event, suggesting that we can infer the effect of a substrate/compound by the presence or absence of the protein of interest rather than know upfront the mechanism *via* which a response is elicited. As we have demonstrated in **Chapter 6 and 7**, the uptake of glutamate *via* EAAT1 induces a change in cell morphology that was triggered by the large influx of $Na^+$ and subsequent cell swelling. While we have only observed this 'phenotype' so far with EAATs, there are at least 60 other SLCs that are coupled to an inward $Na^+$-gradient and, thus, may result in cell swelling or changes in cell morphology upon substrate uptake (**Appendix Table A.2**). For example, $Na^+$-dependent uptake of taurine, glucose and glutamine, among other amino acids, has been associated with cell swelling[122]. In addition, several of these transporters, such as NKCC1 (SLC12A2) and NHE (SLC9 family), are involved in the regulation of cell volume and may be candidates for assessment using impedance[84]. One study reported a label-free assay (dynamic mass redistribution, EPIC) for the $Na^+$-coupled phosphate transporter NaPi-2b (SLC34A2), where stimulation of MDCK-NaPi-2b cells with inorganic phosphate resulted in a positive DMR response[123]. Although the authors did not provide a mechanistic explanation, we may speculate that this response was elicited by $Na^+$-dependent substrate uptake and resultant cell swelling, which could make this transporter amenable for assessment on xCELLigence. It should be noted that **Table A.2** does not include those transporters that are coupled to symport or antiport of other co-substrates[124], which would expand the list substantially.

In addition to changes in cell volume, substrate uptake may disrupt intracellular processes or induce cytotoxicity. Recently, our lab demonstrated that uptake of the neurotoxin

$MPP^+$ in HEK293 JumpIn cells overexpressing organic cation transporters 1–3 (OCT1–3, SLC22A1–3) induces a concentration-dependent impedance response within one hour[125]. Despite the mechanism not being completely understood, we currently hypothesize that $MPP^+$ disrupts the mitochondrial membrane potential, which eventually alters cell morphology. These results indicate a great unexplored potential for SLCs that could be assessed using the label-free approaches described in this thesis. Although the tables in the **Appendix** provide a guideline for the rational selection of SLCs, the best chance to determine whether xCELLigence is suitable for a specific SLC is perhaps the 'phenotypic' approach – add substrate to cells that express the SLC and observe changes in cellular impedance. The HEK293 JumpIn system, with inducible expression of the SLC, may be an excellent starting point to commence these efforts. To help decide whether the next SLC can be tested on xCELLigence, we have provided a illustrative decision tree (**Figure 8.6**).

Fundamental and clinical SLC research has been expanding significantly over the last decades, partly invigorated by community calls that plea for a superfamily-wide approach to deorphanize SLCs and generate reagents, structures and assays[126–128]. The number of SLC drug targets is increasing as well, with several SLCs associated with the development and progression of cancer[129], metabolic disease[99] and neurological disorders[130,131]. For example, the glutamate/cystine antiporter (xCT, SLC7A11) is a promising target for the treatment of various tumors as it plays a role in ferroptosis, tumor growth and chemoresistance[132]. Moreover, the amino acid transporters ASCT2 (SLC1A5) and LAT1 (SLC7A5) are associated to most hallmarks of cancer due to their involvement in energy metabolism[133], and the first small molecule LAT1 inhibitor JPH203 in a clinical Phase I study was well-tolerated and efficacious in patients with advanced solid tumors[134]. In addition, three inhibitors of the glycine transporters (GlyT1/2, SLC6A9/5) are currently in clinical trials for the treatment of cognitive impairment associated with schizophrenia or Alzheimer's disease[135]. Drug discovery and development for these SLCs, in addition to DAT, NET and EAATs, could certainly benefit from the phenotypic impedance-based assays that have been described in this thesis. Altogether, we can conclude that up until now we have barely skimmed the surface of impedance-based assays for SLCs – the prospects for an expansion of the transporter toolbox are good and we may soon welcome this novel platform to the SLC family.

**Final notes**

This thesis describes the development and validation of cell-based label-free assays to assess the function of dopamine, norepinephrine and glutamate transporters. The technology that was used throughout this thesis, xCELLigence, is novel in the field of transporter research and provides an alternative approach to study SLCs. The applications of these assays range from mechanistic investigations to screening of large compound libraries, which could accelerate drug discovery efforts for SLCs. Hopefully, the data presented in this thesis will inspire SLC researchers to rethink transport assays and come up with innovative ways to study this endlessly fascinating family of membrane proteins, which, ultimately, will be lead to improved therapies to the benefit of patients.

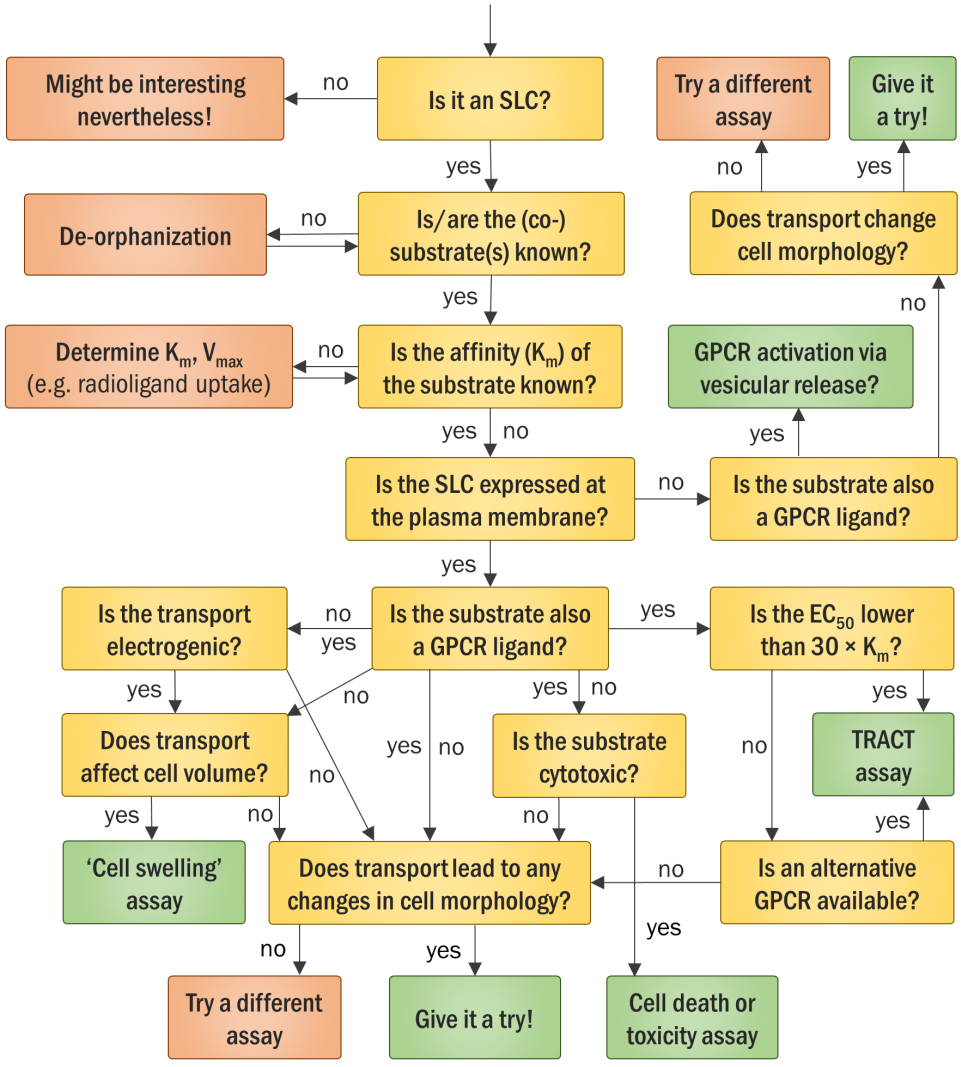


**Figure 8.6** – Decision tree for impedance-based assays for SLCs. Input at the top can be any drug target. Yellow boxes indicate questions. Red boxes indicate decisions that are not related to impedance-based assays. Green boxes indicate impedance-based assays.

## References


1. Bongers, B. J., IJzerman, A. P. & Van Westen, G. J. P. (2019) Proteochemometrics – recent developments in bioactivity and selectivity modeling. *Drug Discov. Today Technol.* **32–33**, 89–98.
2. Burggraaff, L. *et al.* (2019) Identification of novel small molecule inhibitors for solute carrier SGLT1 using proteochemometric modeling. *J. Cheminform.* **11**, 15.
3. Esch, E. W., Bahinski, A. & Huh, D. (2015) Organs-on-chips at the frontiers of drug discovery. *Nat. Rev. Drug Discov.* **14**, 248–260.
4. Langhans, S. A. (2018) Three-dimensional in vitro cell culture models in drug discovery and drug repositioning. *Front. Pharmacol.* **9**, 1–14.
5. Michelini, E., Cevenini, L., Mezzanotte, L., Coppa, A. & Roda, A. (2010) Cell-based assays: Fuelling drug discovery. *Anal. Bioanal. Chem.* **398**, 227–238.
6. Geibel, S., Flores-Herr, N., Licher, T. & Vollert, H. (2006) Establishment of cell-free electrophysiology for ion transporters: Application for pharmacological profiling. *J. Biomol. Screen.* **11**, 262–268.
7. Bazzone, A., Barthmes, M. & Fendler, K. (Academic Press, 2017). SSM-based electrophysiology for transporter research. in *Methods in Enzymology* (ed. Ziegler, C.) vol. 594 31–83.
8. Hillger, J. M., Lieuw, W.-L., Heitman, L. H. & IJzerman, A. P. (2017) Label-free technology and patient cells: from early drug development to precision medicine. *Drug Discov. Today* **22**, 1808–1815.
9. Lundstrom, K. (2017) Cell-impedance-based label-free technology for the identification of new drugs. *Expert Opin. Drug Discov.* **12**, 335–343.
10. Fang, Y. (2011) Label-free biosensors for cell biology. *Int. J. Electrochem.* **2011**, 1–16.
11. Scott, C. W. & Peters, M. F. (2010) Label-free whole-cell assays: Expanding the scope of GPCR screening. *Drug Discov. Today* **15**, 704–716.
12. Doijen, J. *et al.* (2019) Advantages and shortcomings of cell-based electrical impedance measurements as a GPCR drug discovery tool. *Biosens. Bioelectron.* **137**, 33–44.
13. Vázquez-Victorio, G., González-Espinosa, C., Espinosa-Riquer, Z. P. & Macías-Silva, M. (Academic Press, 2016). GPCRs and actin–cytoskeleton dynamics. in *Methods in Cell Biology* (ed. Shukla, A. K.) vol. 132 165–188.
14. Jörg, M. *et al.* (2016) Novel irreversible agonists acting at the A1 adenosine receptor. *J. Med. Chem.* **59**, 11182–11194.
15. Guo, D., Mulder-Krieger, T., IJzerman, A. P. & Heitman, L. H. (2012) Functional efficacy of adenosine A2A receptor agonists is positively correlated to their receptor residence time. *Br. J. Pharmacol.* **166**, 1846–1859.
16. Baltos, J.-A. *et al.* (2017) Capadenoson, a clinically trialed partial adenosine A1 receptor agonist, can stimulate adenosine A2B receptor biased agonism. *Biochem. Pharmacol.* **135**, 79–89.
17. Hillger, J. M. *et al.* (2016) Getting personal: Endogenous adenosine receptor signaling in lymphoblastoid cell lines. *Biochem. Pharmacol.* **115**, 114–122.
18. Nederpelt, I., Vergroesen, R. D., IJzerman, A. P. & Heitman, L. H. (2016) Persistent GnRH receptor activation in pituitary αT3-1 cells analyzed with a label-free technology. *Biosens. Bioelectron.* **79**, 721–727.
19. Hillger, J. M. *et al.* (2015) Whole-cell biosensor for label-free detection of GPCR-mediated drug responses in personal cell lines. *Biosens. Bioelectron.* **74**, 233–242.
20. Linden, J. (1989) Adenosine deaminase for removing adenosine: how much is enough? *Trends Pharmacol. Sci.* **10**, 260–262.
21. Mendel, C. M. & Mendel, D. B. (1985) 'Non-specific' binding. The problem, and a solution. *Biochem. J.* **228**, 269–272.
22. Kenakin, T. P. (1980) Errors in the measurement of agonist potency-ratios produced by uptake processes: A general model applied to β-adrenoceptor agonists. *Br. J. Pharmacol.* **71**, 407–417.
23. Vlachodimou, A., IJzerman, A. P. & Heitman, L. H. (2019) Label-free detection of transporter activity via GPCR signalling in living cells: a case for SLC29A1, the equilibrative nucleoside transporter 1. *Sci. Rep.* **9**, 13802.
24. Zhang, R. & Xie, X. (2012) Tools for GPCR drug discovery. *Acta Pharmacol. Sin.* **33**, 372–384.
25. Cheng, M. H. & Bahar, I. (2019) Monoamine transporters: structure, intrinsic dynamics and allosteric regulation. *Nat. Struct. Mol. Biol.* **26**, 545–556.
26. Kristensen, A. S. *et al.* (2011) SLC6 neurotransmitter transporters: Structure, function, and regulation. *Pharmacol. Rev.* **63**, 585–640.
27. Xue, W. *et al.* (2018) Recent advances and challenges of the drugs acting on monoamine transporters. *Curr. Med. Chem.* **25**, 1–42.
28. Spiegel, S., Maczis, M. A., Maceyka, M. & Milstien, S. (2019) New insights into functions of the sphingosine-1-phosphate transporter SPNS2. *J. Lipid Res.* **60**, 484–489.
29. Prag, H. A. *et al.* (2021) Mechanism of succinate efflux upon reperfusion of the ischaemic heart. *Cardiovasc. Res.* **117**, 1188–1201.

30. Lieb, S. *et al.* (2016) Label-free versus conventional cellular assays: Functional investigations on the human histamine H1 receptor. *Pharmacol. Res.* **114**, 13–26.

31. Sijben, H. J., van den Berg, J. J. E., Broekhuis, J. D., IJzerman, A. P. & Heitman, L. H. (2021) A study of the dopamine transporter using the TRACT assay, a novel in vitro tool for solute carrier drug discovery. *Sci. Rep.* **11**, 1312.

32. Yao, F. *et al.* (1998) Tetracycline repressor, tetR, rather than the tetR–mammalian cell transcription factor fusion derivatives, regulates inducible gene expression in mammalian cells. *Hum. Gene Ther.* **9**, 1939–1950.

33. Butler, R. *et al.* (2015) Use of the site-specific retargeting jump-in platform cell line to support biologic drug discovery. *J. Biomol. Screen.* **20**, 528–535.

34. Zhang, J.-H., Chung, T. D. Y. & Oldenburg, K. R. (1999) A simple statistical parameter for use in evaluation and validation of high throughput screening assays. *J. Biomol. Screen.* **4**, 67–73.

35. Todd, A. C. & Hardingham, G. E. (2020) The regulation of astrocytic glutamate transporters in health and neurodegenerative diseases. *Int. J. Mol. Sci.* **21**, 9607.

36. Doornbos, M. L. J. *et al.* (2018) Constitutive activity of the metabotropic glutamate receptor 2 explored with a whole-cell label-free biosensor. *Biochem. Pharmacol.* **152**, 201–210.

37. Doornbos, M. L. J. *et al.* (2018) Impact of allosteric modulation: Exploring the binding kinetics of glutamate and other orthosteric ligands of the metabotropic glutamate receptor 2. *Biochem. Pharmacol.* **155**, 356–365.

38. Stepanenko, A. A. & Heng, H. H. (2017) Transient and stable vector transfection: Pitfalls, off-target effects, artifacts. *Mutat. Res. Mutat. Res.* **773**, 91–103.

39. Kenakin, T. & Christopoulos, A. (2013) Signalling bias in new drug discovery: Detection, quantification and therapeutic impact. *Nat. Rev. Drug Discov.* **12**, 205–216.

40. Cannon, W. B. (1939) A law of denervation. *Am. J. Med. Sci.* **198**, 737–750.

41. Cannon, W. B. & Rosenblueth, A. (Macmillan, 1949). *The Supersensitivity of Denervated Structures*.

42. Hughes, F. B. & Brodie, B. B. (1959) The mechanism of serotonin and catecholamine uptake by platelets. *J. Pharmacol. Exp. Ther.* **127**, 96–102.

43. Iversen, L. L. (1963) The uptake of noradrenaline by the isolated perfused rat heart. *Br. J. Pharmacol. Chemother.* **21**, 523–537.

44. Iversen, L. L. (1965) The uptake of catechol amines at high perfusion concentrations in the rat isolated heart: a novel catechol amine uptake process. *Br. J. Pharmacol. Chemother.* **25**, 18–33.

45. Schömig, E., Lazar, A. & Gründemann, D. (Springer Berlin Heidelberg, 2006). Extraneuronal monoamine transporter and organic cation transporters 1 and 2: A review of transport efficiency. in *Neurotransmitter Transporters: Handbook of Experimental Pharmacology* (eds. Sitte, H. H. & Freissmuth, M.) vol. 175 151–180.

46. Engel, K., Zhou, M. & Wang, J. (2004) Identification and characterization of a novel monoamine transporter in the human brain. *J. Biol. Chem.* **279**, 50042–50049.

47. Furchgott, R. F. (Springer Berlin Heidelberg, 1972). The classification of adrenoceptors (adrenergic receptors). An evaluation from the standpoint of receptor theory. in *Catecholamines: Handbook of Experimental Pharmacology* (eds. Blaschko, H. & Muscholl, E.) vol. 33 283–335.

48. Fredholm, B. B., Irenius, E., Kull, B. & Schulte, G. (2001) Comparison of the potency of adenosine as an agonist at human adenosine receptors expressed in Chinese hamster ovary cells. *Biochem. Pharmacol.* **61**, 443–448.

49. Wahrheit, J., Nicolae, A. & Heinzle, E. (2013) Investigation of glutamine metabolism in CHO cells by dynamic metabolic flux analysis. *BMC Proc.* **7**, P44.

50. Brabet, I. *et al.* (1998) Comparative effect of l-CCG-I, DCG-IV and γ-carboxy-l-glutamate on all cloned metabotropic glutamate receptor subtypes. *Neuropharmacology* **37**, 1043–1051.

51. Langer, S. Z. & Trendelenburg, U. (1969) The effect of a saturable uptake mechanism on the slopes of dose-response curves for sympathomimetic amines and on the shifts of dose-response curves produced by a competitive antagonist. *J. Pharmacol. Exp. Ther.* **167**, 117–42.

52. Kenakin, T. P. (Elsevier, 2014). *A Pharmacology Primer: Techniques for More Effective and Strategic Drug Discovery. Academic Press* vol. 38.

53. Gesztelyi, R. *et al.* (2012) The Hill equation and the origin of quantitative pharmacology. *Arch. Hist. Exact Sci.* **66**, 427–438.

54. Chi, Y., Suadicani, S. O. & Schuster, V. L. (2014) Regulation of prostaglandin EP1 and EP4 receptor signaling by carrier-mediated ligand reuptake. *Pharmacol. Res. Perspect.* **2**, 1–11.

55. Raffel, D. M. *et al.* (2013) Radiotracers for cardiac sympathetic innervation: transport kinetics and binding affinities for the human norepinephrine transporter. *Nucl. Med. Biol.* **40**, 331–337.

56. Hovde, M. J., Larson, G. H., Vaughan, R. A. & Foster, J. D. (2019) Model systems for analysis of dopamine transporter function and regulation. *Neurochem. Int.* **123**, 13–21.

57. Stein, W. D. (Academic Press, 1986). *Transport and Diffusion Across Cell Membranes*. vol. 1.

58. Vivian, D. & Polli, J. E. (2014) Mechanistic interpretation of conventional Michaelis–Menten parameters in a transporter system. *Eur. J. Pharm. Sci.* **64**, 44–52.

59. Jardetzky, O. (1966) Simple allosteric model for membrane pumps. *Nature* **211**, 969–970.

60. Piniella, D. *et al.* (2018) Identification of novel regulatory partners of the glutamate transporter GLT-1. *Glia* **66**, 2737–2755.

61. Matsson, P. *et al.* (2015) Quantifying the impact of transporters on cellular drug permeability. *Trends Pharmacol. Sci.* **36**, 255–262.

62. Schicker, K., Farr, C. V., Boytsov, D., Freissmuth, M. & Sandtner, W. (2022) Optimizing the substrate uptake rate of solute carriers. *Front. Physiol.* **13**, 817886.

63. Paczkowski, F. A., Bönisch, H. & Bryan-Lluka, L. J. (2002) Pharmacological properties of the naturally occurring Ala457 pro variant of the human norepinephrine transporter. *Pharmacogenetics* **12**, 165–173.

64. Sucic, S. & Bryan-Lluka, L. J. (2002) The role of the conserved GXXXRXG motif in the expression and function of the human norepinephrine transporter. *Mol. Brain Res.* **108**, 40–50.

65. Gu, H., Wall, S. C. & Rudnick, G. (1994) Stable expression of biogenic amine transporters reveals differences in inhibitor sensitivity, kinetics, and ion dependence. *J. Biol. Chem.* **269**, 7124–7130.

66. Reith, M. E. A., Xu, C., Zhang, L. & Coffey, L. L. (1996) Translocation of dopamine and binding of WIN 35,428 measured under identical conditions in cells expressing the cloned human dopamine transporter. *Naunyn. Schmiedebergs. Arch. Pharmacol.* **354**, 295–304.

67. Young, J. D., Yao, S. Y. M., Baldwin, J. M., Cass, C. E. & Baldwin, S. A. (2013) The human concentrative and equilibrative nucleoside transporter families, SLC28 and SLC29. *Mol. Aspects Med.* **34**, 529–547.

68. Vandenberg, R. J. & Ryan, R. M. (2013) Mechanisms of glutamate transport. *Physiol. Rev.* **93**, 1621–1657.

69. Löwe, M., Kalacheva, M., Boersma, A. J. & Kedrov, A. (2020) The more the merrier: effects of macromolecular crowding on the structure and dynamics of biological membranes. *FEBS J.* **287**, 5039–5067.

70. Belo do Nascimento, I. *et al.* (2021) Pharmacological evidence for the concept of spare glutamate transporters. *Neurochem. Int.* **149**, 105142.

71. Scott Ramsey, I. & Defelice, L. J. (2002) Serotonin transporter function and pharmacology are sensitive to expression level. Evidence for an endogenous regulatory factor. *J. Biol. Chem.* **277**, 14475–14482.

72. Chen, N. & Reith, M. E. A. (2007) Substrates and inhibitors display different sensitivity to expression level of the dopamine transporter in heterologously expressing cells. *J. Neurochem.* **101**, 377–388.

73. Shibayama, T. *et al.* (2015) Unstirred water layers and the kinetics of organic cation transport. *Pharm. Res.* **32**, 2937–2949.

74. Korjamo, T., Heikkinen, A. T. & Mönkkönen, J. (2009) Analysis of unstirred water layer in in vitro permeability experiments. *J. Pharm. Sci.* **98**, 4469–4479.

75. Pohl, P., Saparov, S. M. & Antonenko, Y. N. (1998) The size of the unstirred layer as a function of the solute diffusion coefficient. *Biophys. J.* **75**, 1403–1409.

76. Yu, N. *et al.* (2006) Real-time monitoring of morphological changes in living cells by electronic cell sensor arrays: an approach to study G protein-coupled receptors. *Anal. Chem.* **78**, 35–43.

77. Suutari, T. *et al.* (2020) Label-free analysis with multiple parameters separates G protein-coupled receptor signaling pathways. *Anal. Chem.* **92**, 14509–14516.

78. Wootten, D., Christopoulos, A., Marti-Solano, M., Babu, M. M. & Sexton, P. M. (2018) Mechanisms of signalling and biased agonism in G protein-coupled receptors. *Nat. Rev. Mol. Cell Biol.* **19**, 638–653.

79. Christopoulos, A. & Kenakin, T. (2002) G protein-coupled receptor allosterism and complexing. *Pharmacol. Rev.* **54**, 323–374.

80. O'Connor, E. R., Kimelberg, H. K., Keese, C. R. & Giaever, I. (1993) Electrical resistance method for measuring volume changes in monolayer cultures applied to primary astrocyte cultures. *Am. J. Physiol. - Cell Physiol.* **264**, 471–478.

81. Schneider, G. H., Baethmann, A. & Kempski, O. (1992) Mechanisms of glial swelling induced by glutamate. *Can. J. Physiol. Pharmacol.* **70**, S334–S343.

82. Koyama, Y., Sugimoto, T., Shigenaga, Y., Baba, A. & Iwata, H. (1991) A morphological study on glutamate-induced swelling of cultured astrocytes: Involvement of calcium and chloride ion mechanisms. *Neurosci. Lett.* **124**, 235–238.

83. Jakab, M. & Ritter, M. (2006) Cell volume regulatory ion transport in the regulation of cell migration. *Contrib. Nephrol.* **152**, 161–180.

84. Morishita, K., Watanabe, K. & Ichijo, H. (2019) Cell volume regulation in cancer cell migration driven by osmotic water flow. *Cancer Sci.* **110**, 2337–2347.

85. Hoffmann, E. K., Lambert, I. H. & Pedersen, S. F. (2009) Physiology of cell volume regulation in vertebrates. *Physiol. Rev.* **89**, 193–277.

86. Rose, E. M. *et al.* (2009) Glutamate transporter coupling to Na,K-ATPase. *J. Neurosci.* **29**, 8143–8155.

87. Lo, Y. C., Rensi, S. E., Torng, W. & Altman, R. B. (2018) Machine learning in chemoinformatics and drug discovery. *Drug Discov. Today* **23**, 1538–1546.

88. Paul, D. *et al.* (2021) Artificial intelligence in drug discovery and development. *Drug Discov. Today* **26**, 80–93.

89. Liu, X., Ye, K., van Vlijmen, H. W. T., IJzerman, A. P. & van Westen, G. J. P. (2019) An exploration strategy improves the diversity of de novo ligands using deep reinforcement learning: A case for the adenosine A2A receptor. *J. Cheminform.* **11**, 1–16.

90. Schlessinger, A. *et al.* (2018) Molecular modeling of drug–transporter interactions—An International Transporter Consortium perspective. *Clin. Pharmacol. Ther.* **104**, 818–835.

91. Garibsingh, R. A. & Schlessinger, A. (2019) Advances and challenges in rational drug design for SLCs. *Trends Pharmacol. Sci.* **40**, 790–800.

92. Van Westen, G. J. P., Wegner, J. K., IJzerman, A. P., Van Vlijmen, H. W. T. & Bender, A. (2011) Proteochemometric modeling as a tool to design selective compounds and for extrapolating to novel targets. *Medchemcomm* **2**, 16–30.

93. Türková, A. & Zdrazil, B. (2019) Current advances in studying clinically relevant transporters of the solute carrier (SLC) family by connecting computational modeling and data science. *Comput. Struct. Biotechnol. J.* **17**, 390–405.

94. De Bruyn, T. *et al.* (2013) Structure-based identification of OATP1B1/3 inhibitors. *Mol. Pharmacol.* **83**, 1257–1267.

95. Schlessinger, A. *et al.* (2011) Structure-based discovery of prescription drugs that interact with the norepinephrine transporter, NET. *Proc. Natl. Acad. Sci.* **108**, 15810–15815.

96. Schaller, L. & Lauschke, V. M. (2019) The genetic landscape of the human solute carrier (SLC) transporter superfamily. *Hum. Genet.* **138**, 1359–1377.

97. Lin, L., Yee, S. W., Kim, R. B. & Giacomini, K. M. (2015) SLC transporters as therapeutic targets: Emerging opportunities. *Nat. Rev. Drug Discov.* **14**, 543–560.

98. Santer, R. & Calado, J. (2010) Familial renal glucosuria and SGLT2: From a Mendelian trait to a therapeutic target. *Clin. J. Am. Soc. Nephrol.* **5**, 133–141.

99. Schumann, T. *et al.* (2020) Solute carrier transporters as potential targets for the treatment of metabolic disease. *Pharmacol. Rev.* **72**, 343–379.

100. Zhao, S. *et al.* (2019) Linifanib exerts dual anti-obesity effect by regulating adipocyte browning and formation. *Life Sci.* **222**, 117–124.

101. Bhat, S., El-Kasaby, A., Freissmuth, M. & Sucic, S. (2021) Functional and biochemical consequences of disease variants in neurotransmitter transporters: A special emphasis on folding and trafficking deficits. *Pharmacol. Ther.* **222**, 107785.

102. Bai, X. (2021) Progress in structural biology of solute carriers. *Curr. Mol. Biol. Reports* **7**, 9–19.

103. Wright, N. J. & Lee, S.-Y. (2019) Structures of human ENT1 in complex with adenosine reuptake inhibitors. *Nat. Struct. Mol. Biol.* doi:10.1038/s41594-019-0245-7.

104. Nygaard, R., Kim, J. & Mancia, F. (2020) Cryo-electron microscopy analysis of small membrane proteins. *Curr. Opin. Struct. Biol.* **64**, 26–33.

105. Dvorak, V. *et al.* (2021) An overview of cell-based assay platforms for the solute carrier family of transporters. *Front. Pharmacol.* **12**, 1–31.

106. Chivukula, A. S., Suslova, M., Kortzak, D., Kovermann, P. & Fahlke, C. (2020) Functional consequences of SLC1A3 mutations associated with episodic ataxia 6. *Hum. Mutat.* **41**, 1892–1905.

107. Canul-Tec, J. C. *et al.* (2017) Structure and allosteric inhibition of excitatory amino acid transporter 1. *Nature* **544**, 446–451.

108. Canul-Tec, J. C. *et al.* (2022) The ion-coupling mechanism of human excitatory amino acid transporters. *EMBO J.* **41**, e108341.

109. Wu, Q. *et al.* (2022) Ataxia-linked SLC1A3 mutations alter EAAT1 chloride channel activity and glial regulation of CNS function. *J. Clin. Invest.* **132**, e154891.

110. Pant, S., Wu, Q., Ryan, R. & Tajkhorshid, E. (2022) Microscopic characterization of the chloride permeation pathway in the human excitatory amino acid transporter 1 (EAAT1). *ACS Chem. Neurosci.* **13**, 776–785.

111. Kortzak, D. *et al.* (2019) Allosteric gate modulation confers K+ coupling in glutamate transporters. *EMBO J.* **38**, 1–17.

112. Haasen, D. *et al.* (2017) How phenotypic screening influenced drug discovery: Lessons from five years of practice. *Assay Drug Dev. Technol.* **15**, 239–246.

113. Fang, Y. (2015) Combining label-free cell phenotypic profiling with computational approaches for novel drug discovery. *Expert Opin. Drug Discov.* **10**, 331–343.

114. Shih, H. P., Zhang, X. & Aronov, A. M. (2018) Drug discovery effectiveness from the standpoint of therapeutic mechanisms and indications. *Nat. Rev. Drug Discov.* **17**, 19–33.

115. Roshan Moniri, M. *et al.* (2015) Dynamic assessment of cell viability, proliferation and migration using real time cell analyzer system (RTCA). *Cytotechnology* **67**, 379–386.

116. Scott, C. W. *et al.* (2014) An impedance-based cellular assay using human iPSC-derived cardiomyocytes to quantify modulators of cardiac contractility. *Toxicol. Sci.* **142**, 331–338.

117. Peper, J. K. *et al.* (2014) An impedance-based cytotoxicity assay for real-time and label-free assessment of T-cell-mediated killing of adherent cells. *J. Immunol. Methods* **405**, 192–198.

118. Lisby, A. N., Carlson, R. D., Baybutt, T. R., Weindorfer, M. & Snook, A. E. (Academic Press, 2022). Evaluation of CAR-T cell cytotoxicity: Real-time impedance-based analysis. in *Methods in Cell Biology* (eds. Spada, S. & Galluzzi, L.) vol. 167 81–98.

119. Cerignoli, F. *et al.* (2018) In vitro immunotherapy potency assays using real-time cell analysis. *PLoS One* **13**, e0193498.

120. Rashed, M. Z. *et al.* (2021) Rapid detection of SARS-CoV-2 antibodies using electrochemical impedance-based detector. *Biosens. Bioelectron.* **171**, 112709.

121. Pang, Z. P. & Südhof, T. C. (2010) Cell biology of Ca2+-triggered exocytosis. *Curr. Opin. Cell Biol.* **22**, 496–505.

122. Lang, F. *et al.* (1998) Functional significance of cell volume regulatory mechanisms. *Physiol. Rev.* **78**, 247–306.

123. Wong, S.-H., Gao, A., Ward, S., Henley, C. & Lee, P. H. (2012) Development of a label-free assay for sodium-dependent phosphate transporter NaPi-IIb. *J. Biomol. Screen.* **17**, 829–834.

124. Alexander, S. P. H. *et al.* (2021) The concise guide to pharmacology 2021/22: Transporters. *Br. J. Pharmacol.* **178**, S412–S513.

125. Mocking, T., Sijben, H., Vermeulen, Y., IJzerman, A. & Heitman, L. (2022) MPP+-induced changes in cellular impedance as a measure for organic cation transporter (SLC22A1-3) activity and inhibition. *Int. J. Mol. Sci.* **23**, 1203.

126. César-Razquin, A. *et al.* (2015) A call for systematic research on solute carriers. *Cell* **162**, 478–487.

127. Superti-Furga, G. *et al.* (2020) The RESOLUTE consortium: unlocking SLC transporters for drug discovery. *Nat. Rev. Drug Discov.* **19**, 429–430.

128. Hediger, M. A., Clémençon, B., Burrier, R. E. & Bruford, E. A. (2013) The ABCs of membrane transporters in health and disease (SLC series): Introduction. *Mol. Aspects Med.* **34**, 95–107.

129. Pizzagalli, M. D., Bensimon, A. & Superti-Furga, G. (2021) A guide to plasma membrane solute carrier proteins. *FEBS J.* **288**, 2784–2835.

130. Qosa, H. *et al.* (2016) Transporters as drug targets in neurological diseases. *Clin. Pharmacol. Ther.* **100**, 441–453.

131. Aykaç, A. & Şehirli, A. Ö. (2020) The role of the SLC transporters protein in the neurodegenerative disorders. *Clin. Psychopharmacol. Neurosci.* **18**, 174–187.

132. Liu, J., Xia, X. & Huang, P. (2020) xCT: A critical molecule that links cancer metabolism to redox signaling. *Mol. Ther.* **28**, 2358–2366.

133. Lopes, C., Pereira, C. & Medeiros, R. (2021) ASCT2 and LAT1 contribution to the hallmarks of cancer: From a molecular perspective to clinical translation. *Cancers* **13**, 1–26.

134. Okano, N. *et al.* (2020) First-in-human phase I study of JPH203, an L-type amino acid transporter 1 inhibitor, in patients with advanced solid tumors. *Invest. New Drugs* **38**, 1495–1506.

135. Ackermann, T. M., Höfner, G. & Wanner, K. T. (2021) Screening for new inhibitors of glycine transporter 1 and 2 by means of MS binding assays. *ChemMedChem* **16**, 3094–3104.